Fault Detection on Power Cables Based on Ultrasound Images and Fourth-Order Cumulants

by
Huixin Zhang

A Thesis submitted to the Faculty of Graduate Studies of
The University of Manitoba
in Partial Fulfilment of the Requirements for the degree of

Master of Science

Department of Electrical and Computer Engineering
University of Manitoba
Winnipeg

Abstract

Electrical power transmission companies have been inspecting underground power cables in a time consuming and destructive way. The current methodology used by Manitoba Hydro, is to remove the conductive material in the center of the cable, cutting the cable into wafers leaving behind the insulating polymer material known as XLPE, the area where many faults occur, and inspect the wafers manually with a microscope. The main goal of this work was to find a methodology to detect these cable faults in a non-destructive way so that the quality of the cable may be assessed, and its remaining lifetime be estimated and return it to use if possible. Two XLPE power cable samples were tested. Three small holes were drilled in one XLPE cable. A capacitive transducer with center frequency of 802.8 kHz was applied for transmitting receiving signal. For each sample, 48 scans were collected. Based on ultrasound images, we were able to detect these faults in this XLPE material from the peaks of the samples corresponding to the XLPE area by setting a threshold to 0.08 volts. Also, this detection technique was improved by using fourth-order cumulants.

Acknowledgements

This thesis would not have been possible without the help of so many people in various ways. First of all, I would like to express my deepest gratitude to my advisor, Prof. Thomas Gabriel for guiding and supporting me over the years. I have been so fortunate to have such an advisor with great motivation and immense knowledge. Prof. Thomas directed me to the way for research all the time and helped me with writing this thesis. I greatly appreciated his encouragement which boosted my enthusiasm towards signal processing and all related research works.

Besides, I would like to thank the rest of my thesis committee for their invaluable discussion, ideas and feedback. I would like to thank all the professors in the department in Electrical and Computer Engineering and other departments at the University of Manitoba for their well-taught lectures. Also, my sincere thanks go to the technicians Mount First and Guy Jonatschick. What is more, I would like all my colleagues Jose J. Mijares Chan, Rui Zhang and Binglin Li for all our valuable discussions in research and boundless friendship during the past two years.

Finally, I would like to thank my amazing family for the love, support, and encouragement I have gotten over the years. In particular, I would like to thank my parents, my husband and my son. Undoubtedly, I could not have done this without you.

Contents

Abstract ii
Acknowledgements ii
List of Figures v

1 Introduction **1**
1.1 Background and Motivation 1
1.1.1 Cable Insulation Materials 1
1.1.2 Water Tree 3
1.1.3 The Method Applied by Manitoba Hydro for Detecting Water Trees 4
1.2 Non-Destructive Testing 5
1.2.1 Motivation 7
1.3 Summary of Contributions 8
1.4 Outline of the Thesis 9

2 Non-destructive Testing Using Ultrasound **10**
2.1 Basic Knowledge of Sound 11
2.1.1 Characteristics of Sound 11
2.1.2 Modes of Propagation 12
2.1.3 Wavelength and Defect Detection 13
2.2 Interactions of Ultrasound with Materials 14
2.2.1 Acoustic Impedance 14
2.2.2 Reflection 15
2.2.3 Refraction and Scattering 15
2.2.4 Attenuation 16
2.3 Ultrasonic Transducer 17
2.3.1 Ultrasonic Modes 17
2.3.2 Types of Air Coupled Transducers 18
2.3.3 Transmitter and Receiver Operation of Capacitive Transducer . . . 19
2.4 Principles of Capacitive Transducer 20
2.4.1 A Capacitor 20
2.4.2 Capacitance 21
2.4.3 Dielectric Constant 22
2.4.4 Capacitive Transducer Applications 22
2.5 Image Data Acquisition 23
2.5.1 Signal Generator 23
2.5.2 Pulse-Echo Operation 24

2.5.3 Echo Display Methods 25

3 A Non-linear Signal Processing Framework: Higher Order Spectra Analysis 27
3.1 Power Spectrum 28
3.2 Polyspectra 29
3.3 High-order Cumulants 30
3.3.1 Definition of kth-order Cumulant and Polyspectra 30
3.3.2 Bias, Variance and MSE of an Estimator 31
3.3.3 Estimating Cumulants and Polyspectra 32
3.4 Higher Order Spectral Analysis Toolbox 33
3.5 Analysis of Ultrasound Scans Based on Higher Order Cumulants 34

4 Fault Detection on Power Cables Based on Ultrasound Images and Higher Order Spectra 37
4.1 Instrumentation Setup 37
4.1.1 Introduction of the Instruments 38
4.1.2 System Setup 40
4.2 Test the System 41
4.3 Data Collection 42
4.3.1 Generate the Transmitted Signal 42
4.3.2 Collect Received Scans from Transducer 45
4.4 Results 47
4.4.1 The Results Based on Ultrasond Image 47
4.4.2 The Results Based on Fourth-order Cumulants 51

5 Conclusions and Future Work 60
5.1 Conclusion and Comments 60
5.2 Future Work 61

References 63

List of Figures

1.1 (a) Typical low voltage PVC cable [2]. (b) Low voltage/medium voltage PE cable for outdoor usage [2]. 2
1.2 Basic construction of multi-core XLPE insulation cable. 3
1.3 (a) Dissection of underground cable into thin wafers [16]. (b) Wafer as seen without a microscope. A paper clip at the top of the image points to the water tree [16]. (c) Video-microscope [16]. 5
1.4 Ultrasound flaw detector, cable and casing used in [16]. 7

2.1 Longitudinal wave which was used in the test. 12
2.2 Shear wave 13
2.3 Reflection and refraction of ultrasound occur at material boundaries with differences in acoustic impedance. 16
2.4 The assembly of a signal-element capacitive ultrasound. 19
2.5 Capacitor used in a circuit to store electrical charge. 21
2.6 Transmitted waveform used. 24
2.7 A-Scan presentation [59]. 26

3.1 The polyspectra classification map. 29
3.2 (a) Sine burst (3 cycles) with Gaussian noise added, (b) Sine burst (1 cycle) with Gaussian noise added, (c) Fourth-order cumulants of the signal in (a), peak = -33.07 db, (d) Fourth-order cumulants of the signal in (b), peak = -36.2496 db, (e) Third-order cumulants of the signal in (a), peak = -39.25 db,(f) Third-order cumulants of the signal in (b), peak = -39.41 db. 35

4.1 Ultrasound equipment set up used in this work (1 oscilloscope, 2 ultrasonic transducer, 3 function generator, 4 remote module and hub unit, 5 power amplifier.) 38
4.2 (a) Function generator. (b) Oscilloscope. 39
4.3 (a) Power amplifier. (b) Remote module unit. (c) Control hub. (d) Transducer. 39

4.4 Ultrasound transducer characterization. 40
4.5 (a) Two examples of data collected with no foreign object at the center of the cable. (b) Another two examples when a metal cylinder was placed at the center. Note the difference on waveforms received for the two different cases. 42
4.6 (a) Two examples of data collected with a red cable beneath the transducer. (b) Another two examples when there is no cable under the transducer. Note the difference on waveforms received for the two different cases. . . . 43
4.7 (a) The time difference between the transmitted signal and the first highest peak of the received scan. (b) The distance between the transducer and the surface of the red cable. 44
4.8 Transmitted signal. 45
4.9 Picture of cables under test. (a) Good cable. (b) Bad cable. 45
4.10 OpenChoice Desktop. 46
4.11 Logitech webcam for image acquisition. 48
4.12 The difference between the two received scans when there is cable and no cable. 48
4.13 Original scans with first highest amplitudes. 49
4.14 Picture of the cable under test as well as the measured sound velocities of the different layers that are on top of the XLPE insulation. 50
4.15 (a) Samples within XLPE area. (b) Position14. (c)Position 17. (d)Position 37. 52
4.16 Peaks of the original data for the 48 scans (faulty cable). Except for the peaks of position 14, 17 and 37, none of the other peaks reaches the threshold 0.08. 53
4.17 Original samples within XLPE of position 37. 53
4.18 Samples of original received signal within XLPE for good cable. 55
4.19 Peaks of the original data for the 48 scans (good cable). None of the peaks reaches the threshold 0.08. 55
4.20 (a)(b) Fourth-order cumulants of received signal from position 4 and position 21 with no faults in the LOS of transducer. (c) Fourth-order cumulants of received signal from position 14 where there are 2 holes in the LOS of transducer. (d)Fourth-order cumulants of received signal from position 37 where there is 1 hole in the LOS of transducer. 56
4.21 Peaks of fourth-order cumulants of 48 scans for the faulty cable. 57

4.22 Original samples within XLPE of position 17 with two holes in the LOS of transducer and original samples within XLPE of position 37 with one hole in the LOS of transducer. 57
4.23 Original scans of position 21 (no hole) and position 37 (one hole). The peak of scan 37 is 3.56 decibels higher than the peak of scan 21. 58
4.24 Peaks of fourth-order cumulants results of 48 scans for the good cable . . . 58

Chapter 1

Introduction

1.1 Background and Motivation

1.1.1 Cable Insulation Materials

Generally speaking, safety and reliability have been considered as the two most important factors in manufacturing electric power cables. In the matter of insulation materials, they must possess impressive electrical and physical properties. In the past, wiring cables had been insulated with vulcanized natural rubber (VIR), dry paper, polyvinyl chloride (PVC) or polyethylene (PE) [1]. PVC is cost effective, durable and widely available, therefore, it is the most commonly used insulator for cables. Nevertheless, due to its limited thermal capability, the normal operating temperatures are typically between 75 celsius degree and 105 celsius degree depending on the types of PVC [2]. In addition, the chlorine in PVC leads to thick, toxic and black smoke when burnt, which is hazardous to health in some confined areas such as tunnels [3]. Another generally used insulator is PE. Compared with PVC, PE is much lighter and has lower dielectric losses. More importantly, even though the insulation thickness of PE is less than PVC, PE cables present better mechanical and insulating characteristics including moisture resistance, insulation resistance, chemical resistance, abrasion resistance, cut-through resistance, elongation and rodent resistance.

However, PE is highly sensitive to water treeing and the material breaks down at high temperature [2]. PVC and PE cables are shown in Figure 1.1. None of them could meet the increasing demands for underground electric power until 1955, when the Cross-linked Polyethylene, known as XLPE, was first accomplished at the GE Research Laboratory [1].

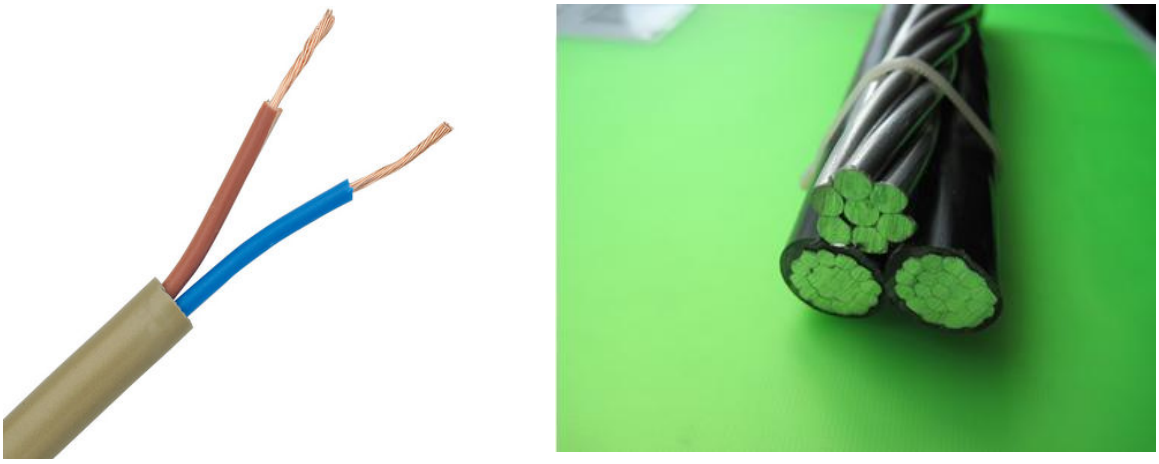

(a) (b)

Figure 1.1: (a) Typical low voltage PVC cable [2]. (b) Low voltage/medium voltage PE cable for outdoor usage [2].

The effect of the cross-linking is to prohibit the movement of molecules from each other under the stimulation of heat by applying small amount of chemical additives. This enables XLPE to be resistance to long term exposure to high temperature and chemical corrosion, and exhibit high current carrying capacity over the full temperature range. Also, XLPE has light weight, small bend radius, hence saving installation cost. All these features have given rise to the rapid growth of preference for XLPE cables in the electrical industry.

The basic construction of XLPE cable is similar to PVC cable, as shown in Figure 1.2. The only difference is the insulation material. The conductor screen is a thin layer extruded in the same operation as the insulation and cross-linked with it so that the two components are closely bonded. Generally, single-core and three-core designs are employed, and there is a scope for constructional variation depending on the condition of use, subject to the cores being surrounded individually or as a three-core assembly by a metallic layer [4].

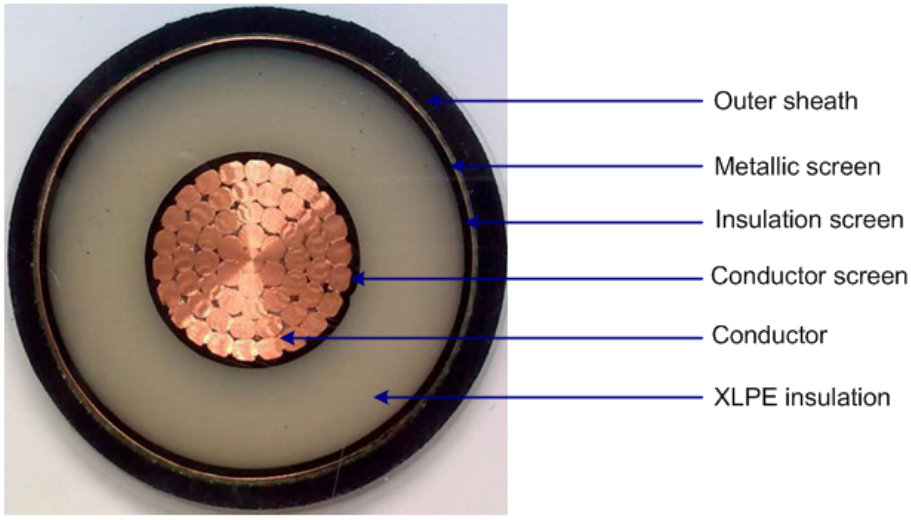

Figure 1.2: Basic construction of multi-core XLPE insulation cable.

1.1.2 Water Tree

The reliability of XLPE cables decreases with time as a result of the degradation of the XLPE insulation material. One of the most critical reasons is the occurring of water trees within the XLPE insulation which were first encountered in Japan [5], and they can result in distribution failure. Numerous water treeing studies have been carried out during the 1970s, 1980s and 1990s [6]. Various researchers have concluded that the main causes of water trees are field driven oxidation and electric field-induced chemical reaction [7–10].

Water treeing is regarded as a degradation phenomenon creating structures in insulation material under the influence of moisture and an electric field [10]. Based on the initiation mechanism, water trees are classified into two types: vented trees and bow-tie trees. Vented trees grow from either side of the insulation material to the other side. The origins could be mechanical damage to the insulation material or be irregular contact between the semiconductor screen and the insulation material [11]. Bow-tie trees initiate from the inside of the insulation and grow towards the boundaries.

Water trees are constituted by numerous voids which are filled with non-polymeric substance. The structure of voids including size, connectivity, density, length and growth rate has aroused researchers's great interest. However, it is difficult to reach a consensus on

the structure knowledge. The two main reasons are that the voids collapse on drying and sectioning of cables results in structures distortion [12]. Even so, the fact that either the number or size of the voids increases with water tree growth was demonstrated in a variety of studies of water content in trees [13, 14].

The XLPE with water trees is still a good insulator, but has lower resistance to discharge. However, water trees grow and may eventually lead to electric failure when they bridge the outer ground layer to the center high voltage conductor. Also, an electric tree could be initiated if the stress across the insulation exceeds the reduced discharge resistance of the water tree [15], which results in complete insulation breakdown.

Since this phenomenon weakens the performance of XLPE insulation and jeopardizes the multi-billion dollar utility investment in power cables, a number of experiments have been conducted for locating the water trees in XLPE cables.

1.1.3 The Method Applied by Manitoba Hydro for Detecting Water Trees

As the water trees degrade the integrity of XLPE insulation and decrease the power system reliability, detecting water trees has been an effective preventive maintenance method. Field staff take the number and length of the trees into consideration when they decide to replace the cable. The current methodology used by Manitoba Hydro is dissection which consists of the following steps [16]:

- A 6-inch length cable is removed from a failed sample received from the field.
- The conductor is removed from this section.
- A specific woodworking miter slices the cable into 1.00-mm thick wafers.
- The wafers are boiled in water for one hour so as to identify and measure the water trees better
- The wafers are analyzed under a video-microscope, as shown in Fig. 1.3 (c).

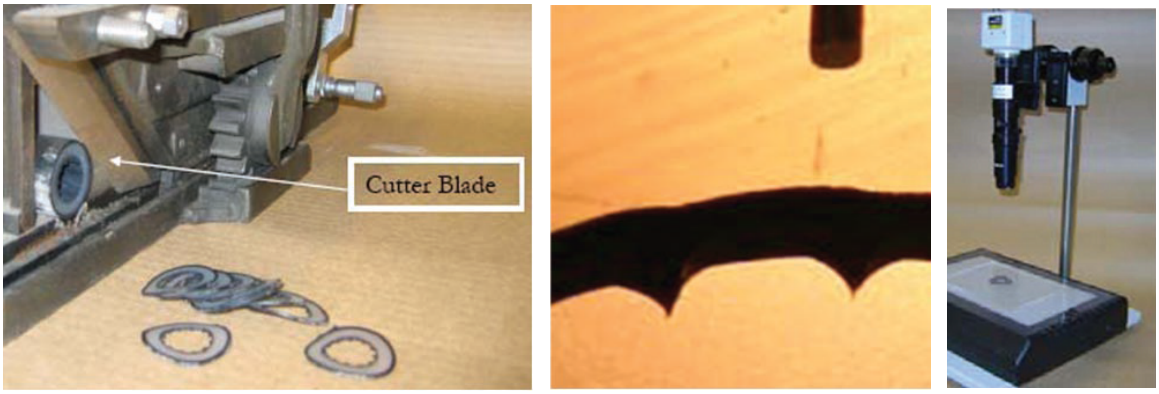

(a) (b) (c)

Figure 1.3: (a) Dissection of underground cable into thin wafers [16]. (b) Wafer as seen without a microscope. A paper clip at the top of the image points to the water tree [16]. (c) Video-microscope [16].

Manitoba Hydro inspects XLPE underground power cable in a time consuming and destructive way. Therefore, this thesis proposes a more effective method for detecting the water trees.

1.2 Non-Destructive Testing

Non-destructive testing (NDT), as the name implies, refers to a technology that does not damage or alter the materials being tested. This method includes X-ray inspection, optical imaging, nuclear magnetic resonance (MNR), ultrasonics, and the like. All of them have been used in detecting water trees in power cables. When field staff decide which method is the best choice, the factors of speed, accuracy, cost and complexity are generally taken into account.

- *X-ray Inspection*: X-radiation which is composed of X-rays is a form of electromagnetic radiation. X-rays are classified into soft X-rays and hard X-rays based on the energy amplitude of energy. With lower penetration ability, soft X-rays are used for thickness gauges and for X-ray fluoresces [17] to determine chemical composition. Hard X-rays can be used to penetrate relatively thick objects. A 3-D replica using X-ray computed tomography (XCT) imaging technique with phase

contrast enhancement has been proposed for water tree analysis and detection [18]. With the frequencies in the range of 30 petahertz to 30 exahertz, X-rays are easily absorbed in air. Also, there are health issues to consider, especially with hard X-rays or gamma sources.

- *Optical Imaging*: Optical NDT has become more and more widely used in recent years due to its non-destructive imaging characteristics with high precision and sensitivity. The main optical NDT technologies include fibre optics, electronic speckle, infrared themography, endoscopic and terahertz technology [19]. Optical imaging is commonly used for validating dimensions of parts or products, assessing the correct placement of labels on a package or inspecting samples for defects. In terms of detecting water trees, much information such as the shape, the fractal dimension and the tree length can be extracted from 2-D optical images. Nevertheless, optical methods tend to be limited by the resolution which refers to the closest two points that can be resolved [18].

- *Nuclear Magnetic Resonance*:NMR relies on a strong DC magnetic field and a high frequency radio wave that is used to probe the chemical composition of a sample. NMR methods for industrial applications are used to monitor the chemical composition of samples. Usually test samples are removed from a production batch for analysis. It was applied to detect water trees in low density polyethylene cables and the result showed drastic changes in the unaffected and affected regions [20]. NMR methods are well proven and reliable, however they may not provide instantaneous feedback in an on-line process. The time required to remove and analyze a sample may be costly.

- *Ultrasonics*: Ultrasound technology was introduced by Auckland et Al. [21] based on the use of a back propagation neural network. This approach used a commercial ultrasonic flaw detector to produce A-scans of the insulation material. A PC scanner system was developed so that the insulation could be mapped according to the signal

depth or amplitude [21]. The acoustic emission equipment was a standard commercial system with a 10 MHz probe. Using a 10 MHz ultrasound system, cavities inside the cable containing air and water with dimensions ranging from 20 to 300 (m) were detected. Although water tree related flaws were accurately characterized, no imaging was performed due to the limited computational capabilities of the data acquisition equipment available at the time of the study [22, 23]. Additionally, no imaging was reported on actual power cables. At the University of Manitoba, a successful imaging system based on also a 10 MHz system and synthetic aperture imaging was developed to image faults of up to 1 mm on a power cable [16]. Figure 1.4 shows the system used in [16].

Figure 1.4: Ultrasound flaw detector, cable and casing used in [16].

1.2.1 Motivation

The motivation of this thesis is mainly concentrated on the following aspects:

The main goal of the project was to find a methodology to detect these cable faults in a non-destructive way so that the quality of the cable may be assessed, and its remaining lifetime be estimated and return it to use if possible. One major challenge faced was that

the cable length could be up to 100 meters. This requirement made the feasibility of using water immersion inspection, often used in ultrasound imaging, impractical, as a water tank facility would require submersion of at least a significant portion of the cable. This would also require a precise rotation motion of either the cable and/or the sensors. The system shown in Figure 1.4 poses the challenge of using a considerable amount of ultrasonic gel to inspect the entire cable.

Another substantial challenge not related to the water submersion system, was the attenuation of the ultrasound pulse in the cable, which was especially aggravated by the three layers of the cable on top of the XLPE insulation, in which the faults are normally found. The interface between each of the different layers presents a loss and reflection of acoustic power arising from the different acoustic impedance of each of the layers. As such, it was difficult to obtain substantial acoustic power to reach the XLPE section of the cable that was not severely corrupted by noise. This is the reason why in [16] the outer layer of the cable was removed. Furthermore, the acoustic attenuation increases, limiting the acoustic power as the acoustic frequencies are increased. Therefore, with the higher frequencies, needed for high-resolution imaging, the attenuation worsens.

1.3 Summary of Contributions

The contribution of this thesis are summarized as follows:

In Chapter 4, the methodology of fault detection on XLPE power cables based on ultrasound images and the fourth-order cumulants is proposed. The main hardwares include function generator, oscilloscope, power amplifier, control hub, remote module unit and ultrasonic transducer. The capacitive transducer developed by VN Instruments has superior bandwidth and very good sensitivity and stability over time. We concentrated our efforts on developing ultrasound technology with frequencies in the range of 600 KHz to 1 MHz that could detect faults of up to 1.5 mm in size and yet that could offer inspection on air without the need of a water immersion system or copious amounts of ultrasonic gel. Two

types of XLPE cables have been tested. In order to detect the holes from the received A-scans, a threshold was set and none of the peaks reached it except those corresponding to the positions of holes. Also, a simple signal processing solution was developed to enhance the detection of these faults. Once the potential areas of the cable have been highlighted with such a system, a similar analysis as presented in [16] or even the analysis discussed in Figure 1.3 can be used to assess the amount of damage, this in a destructive way but knowing before-hand that there are problems in that section of the power cable.

1.4 Outline of the Thesis

The rest of the thesis is organized as follows. Chapter 2 introduces the most important technology related to our research. Motivated by the limits of Manitoba Hyrdo's existing methods for detecting water trees in XLPE cables, the non-destructive testing using ultrasound transducer is described, including basic knowledge of sound, interactions of ultrasound with materials, ultrasound transducer, principles of capacitive transducer and image data acquisition. Chapter 3 states the theory of high-order spectrum which was used in this work to further locate the flaws in the sample cables. In Chapter 4, the detailed process of the experiment is described and the results are analyzed. Finally, Chapter 5 summarizes a brief conclusion of this thesis and indicates some future work.

Chapter 2

Non-destructive Testing Using Ultrasound

Ultrasound is the term that describes sound waves with frequencies from 20 kHz up to several gigahertz which is beyond the upper audible limit of human hearing. Ultrasound is not harmful to the subject to be tested nor the person conducting the test. In addition, it is more economical than many other similar testing methods (e.g. X-ray methods) and easy to be produced. Due to these advantages, it has been widely used in medicine as well as industry. In recent decades, many researchers have performed experiments to prove that ultrasound is an effective technique which can be used for fault detection in many materials [24]. In this chapter, the method of non-destructive testing (NDT) using ultrasound is presented as the basis for the work. The basic knowledge including characteristics of sound, modes of propagation and wavelength's role in defect detection is described, followed by the principles of interactions of ultrasound with materials, ultrasonic transducer and image data acquisition.

2.1 Basic Knowledge of Sound

Sound is mechanical energy and it results from propagating through a continuous, elastic medium by the compression and rarefaction of "particles" that comprise it.

2.1.1 Characteristics of Sound

Sound is commonly characterized by three properties: wavelength, frequency and velocity.

- *Wavelength*: The wavelength of sound (λ) is defined as the distance between the analogous points of two successive waves. Any type of wave has a corresponding wavelength, and it is considered as a limiting parameter for controlling the information content that can be derived from the behavior of a wave [25].

- *Frequency*: The frequency (f) is the number of complete back-and-forth vibrations of a particle of the medium each second. Usually, we use Hertz (abbreviated Hz) as the unit for frequency. Sound waves with frequencies less than 20 Hz are referred to as infrasound. The generally stated range of audible frequencies is 20 Hz to 20 kHz. And ultrasound represents the frequency range above 20 kHz. The period is the time duration of one wave cycle. It is inversely related to frequency and is equal to $1/f$.

- *Velocity*: The velocity of sound is the distance traveled by the wave propagating through a medium per unit time. It is determined by the characteristics of the material instead of the characteristics of the sound and it is different in various materials. The reason is that the sound wave is produced due to the vibration of particles within a material and the velocity of sound depends on the elastic constant and material density. It can be obtained by the following equation [26]

$$V = \sqrt{\frac{C}{\rho}} \tag{2.1}$$

where C is the elastic constant and ρ is the material density. Both of the two parameters are different for different materials.

The relationship between wavelength, frequency and speed of sound is

$$c = \lambda f \tag{2.2}$$

where $c(m/s)$ is the speed of sound in the medium, $\lambda(m)$ is the wavelength, and $f(Hz)$ is the frequency.

2.1.2 Modes of Propagation

According to the way particles oscillate, sound waves propagate in four principal modes: longitudinal waves, shear waves, surface waves and plate waves. The two types of waves that are widely used are longitudinal waves and shear waves. Also, they are the most common waves employed in ultrasonic flaw detection [27].

- *Longitudinal Waves*: A longitudinal wave is characterized by a fixed point moving parallel with the wave motion, as from a piston source. They are also called pressure or compression waves because compression and expansion forces are active in these waves [28].

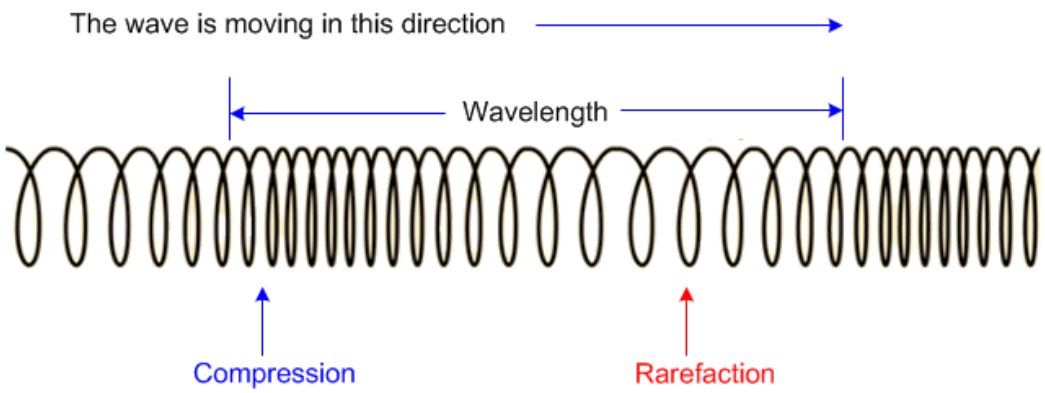

Figure 2.1: Longitudinal wave which was used in the test.

- *Shear Waves:* A shear wave, also known as transverse wave, is characterized by particle motion transverse to the direction of wave propagation. Shear waves can propagate through solid materials because they have enough shear strength [29], therefore, they can not effectively propagate in materials like liquids or gases.

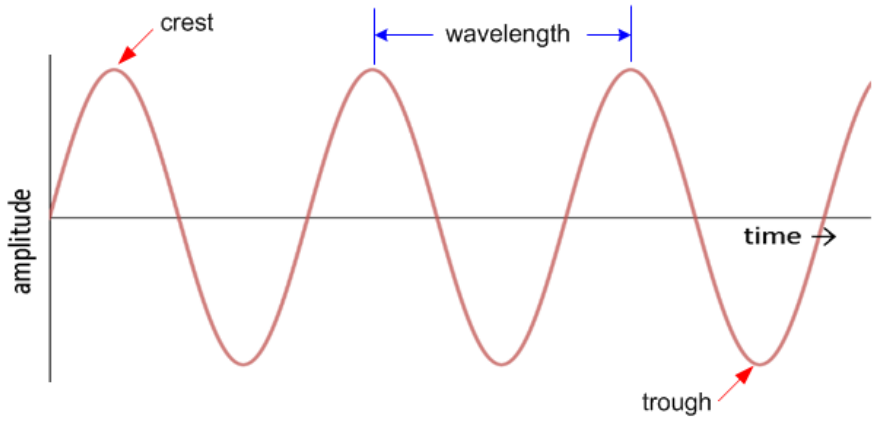

Figure 2.2: Shear wave

As mentioned previously, longitudinal and shear waves are most often used in ultrasonic detection. However, as there are different types of elliptical or complex vibrations of the particles at materials' surfaces or interfaces, it makes other waves possible, some of which such as rayleigh waves and lamb waves [30] are also useful for ultrasonic detection. In this work, longitudinal waves were used.

2.1.3 Wavelength and Defect Detection

The velocity of sound waves in a certain medium is fixed. Hence, it can be noted from the equation 2.2 that an increase in wavelength will result in a decrease in frequency.

The wavelength of the ultrasound signal plays an important role in the probability of detecting a discontinuity. Generally, the accepted lower limit of detection for a small flaw is one-half wavelength [31]. Any flaw smaller than that will be invisible. This ability is called sensitivity, which is a term that is often used in ultrasonic detection to evaluate a technique's ability to locate flaws. It increases with shorter wavelengths. Another important term is

resolution, which is the ability of locating flaws close together within the material. It also increases with shorter wavelength. Hence, from the two aspects, a shorter wavelength is preferable.

As we have discussed previously, with fixed velocity, frequency is inversely proportional to wavelength. Therefore, a high-frequency ultrasound beam (small wavelength) provides better resolution and image details than a low-frequency beam. However, attenuation increases with higher frequency [32] and consequently, the maximum depth in a material that flaws can be detected is significantly reduced. Thus, in ultrasonic testing, the inspector must take a range of factors into account when making a decision about the ultrasound frequency.

2.2 Interactions of Ultrasound with Materials

As ultrasound propagates through different mediums, interactions including reflection, refraction, scattering and absorption occur. These interactions are determined by the acoustic properties of matter.

2.2.1 Acoustic Impedance

The acoustic impedance (Z) of a material is the ratio of acoustic pressure to flow [33]. It is defined as

$$Z = \rho c \tag{2.3}$$

where ρ is the density in kg/m^3 and c is the velocity of sound in m/s. The SI unit of acoustic impedance is $kg/(m^2 s)$ and $rayl$.

Acoustic impedance plays an important role in the determination of acoustic transmission and reflection at the interface of two materials having different acoustic impedances [34], which is the primary principle for detecting faults using pulse-echo techniques.

Table 2.1: REFLECTION AND TRANSMISSION COEFFICIENTS OF MATERIALS USED IN THIS WORK [36]

Interface	Reflection coefficient	Transmission coefficient
$Air - Acrylic$	99.959%	0.041%
$Air - SS^a$	99.959%	0.041%
$SS - XLPE^b$	0.861%	99.139%
$XLPE - Air$	99.912%	0.088%

a. Semiconductive screen
b. Cross-linked polyethylenee

2.2.2 Reflection

Reflection results from the difference in the acoustic impedance of adjacent materials, which is referred to as the impedance mismatch. The greater impedance mismatch leads to greater percentage of energy that will be reflected at the interface between two materials. The reflected fraction of sound intensity incident on an interface is usually described by the reflection coefficient [35], which is expressed as

$$R_i = \left(\frac{Z_i - Z_{i-1}}{Z_i + Z_{i-1}} \right)^2 \tag{2.4}$$

where Z_i is the acoustic impedance of the i^{th} medium.

The i^{th} transmission coefficient T_i is simply equal to $1 - R_i$. Both transmission and reflection coefficients were calculated from the acoustic impedances of the materials involved in this work and the corresponding values can be found in Table 2.1. In order to get these values, a Micrometries 1305 Multi-volumn pycnometer was used to measure the density and the thickness of the material and the time of traveling from one interface to the other was used to calculate the velocity of sound [36].

2.2.3 Refraction and Scattering

When the beam is not perpendicular to the boundary of different materials, the direction of the transmitted ultrasound energy changes, which is called refraction. The angle is determined by the change in velocity of sound, and the relationship is described by Snell's

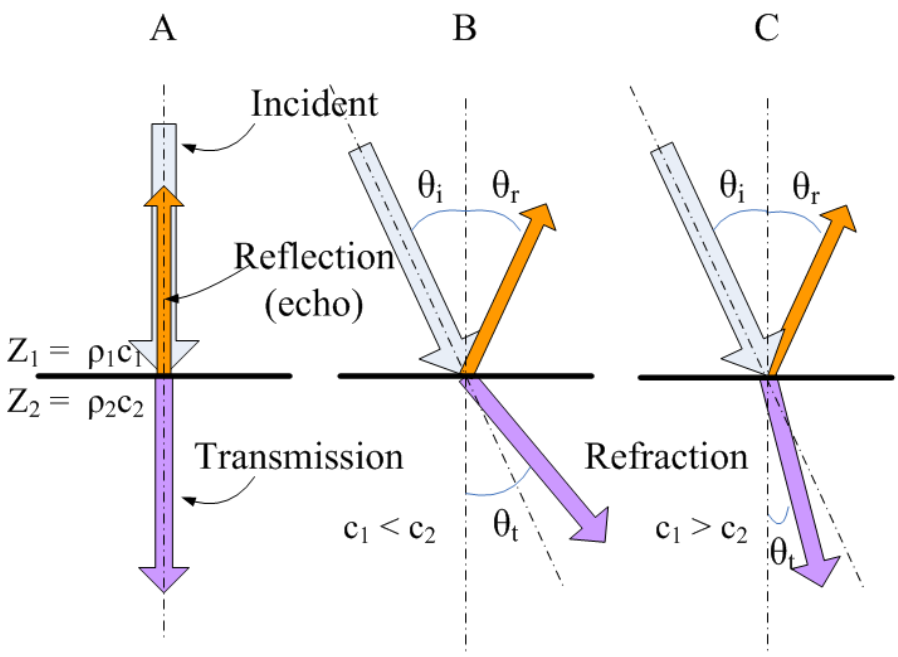

Figure 2.3: Reflection and refraction of ultrasound occur at material boundaries with differences in acoustic impedance.

Law

$$\frac{sin(\theta_i)}{c_1} = \frac{sin(\theta_r)}{c_2} \tag{2.5}$$

where θ_i and θ_r are incident and refraction angle respectively, c_1 and c_2 are sound velocities in the medium. Nevertheless, the frequency of ultrasound remains the same when propagating through various materials.

Specular reflection occurs at flat, smooth boundaries and the direction only depends on the angle of incidence. However, there are two conditions that result in scattering. The first one is when the incident wave encounters a boundary that is not perfectly flat or smooth, and the second one is when the wavelength of the ultrasound wave is larger than the dimensions of the reflective objects.

2.2.4 Attenuation

As an ultrasound wave travels within a material, attenuation of acoustic energy happens, which is mainly caused by scattering and material absorption of the incident beam. The

attenuation coefficient μ is expressed in units of dB/m, with the physical meaning of relative intensity loss per meter for a given medium. Then the amplitude can be expressed as

$$A = A_0 e^{-\mu z} \tag{2.6}$$

where A is the attenuated amplitude after the wave traveling a distance z, A_0 is the original amplitude of the wave, μ is the attenuation coefficient and z is the travel distance.

The attenuation coefficient of the signal in the XLPE cable is fairly constant with the value 0.02 dB/m if the frequency is below 10 MHz. And this parameter becomes frequency-dependent at higher frequencies [37]. In this work, the frequency of ultrasonic transducer is below $10MHz$ and the distance between the surface of the cable and the boundary of the conductor and XLPE is around 15 mm, therefore, the attenuation is almost ignorable.

2.3 Ultrasonic Transducer

Ultrasound is transmitted and received with an ultrasonic transducer, which is an electronic device that converts ultrasound waves into electrical waves or vice versa.

2.3.1 Ultrasonic Modes

Commonly, there are three ways of sending ultrasonic signals through an object: contact ultrasonics, immersion ultrasonics and air-coupled ultrasonics.

- *Contact Ultrasonics*: Contact transducers are designed for use in direct contact with test subjects. Coupling gel is applied to remove the air gap between the transducer and the object so that the transducer is able to transmit a strong and clear signal.
- *Immersion Ultrasonics*: Immersion transducers do not touch the objects directly. They are typically immersed inside water that is used as a coupling medium to alleviate the impedance mismatch between the transducer and the objects. Nevertheless,

water may cause damage to some material like wood, paper, plastics and so on. Also, the use of water reduces the flaw detection probabilities in porous materials [38].

- *Air Coupled Ultrasonics*: As the name indicates, this method relies on the air or another gas to enable the waves to reach test objects, thereby avoiding using direct coupling or liquid coupling.

2.3.2 Types of Air Coupled Transducers

The technique of using air coupled transducers for ultrasonic imaging has given rise to the interest in designing better transducers. Typically, transducers are classified according to the physical principles which permit the radiation of ultrasound. Researchers have investigated a range of transducers including electrostatic, electrodynamic, magnetostrictive, piezoelectric and pneumatic transducers [39]. However, piezoelectric transducers are the most common and electrostatic (capacitive) transducers are becoming a topic of research lately.

- *Piezoelectric*: The primary component of the transducer is the piezoelectric material which is often a crystal or ceramic. It converts electrical energy into sound energy for ultrasound generation and sound energy into electrical energy for ultrasound detection by physical deformation of the structure [40]. The main problem is that the impedance mismatch at the piezoelectric/air boundary is large. Hence, the backing block and matching layers with a quarter wavelength determined by the center frequency of the transducer are applied to improve the transmission coefficient [41]. An alternative method is to modify the piezoelectric material by using a ceramic/polymer composite. However, they all operate over a narrow bandwidth and are usually designed for a specific application [42].

- *Capacitive*: Another form of air coupled transducer is the capacitance design [42]. Essentially, a capacitive transducer is a parallel-plate capacitor with one rigid immovable electrode (the solid backplate) and one flexible movable electrode

(the polymer membrane). Small pockets of trapped air between the backplate and membrane improve the coupling to the air. Due to the small thickness and mass of the membrane, the capacitive transducer has a much greater bandwidth than the piezoelectric transducer. Also, direct current bias voltage is applied so that the membrane is attracted to the backplate [43], as shown in Figure 2.4. In light of its advantages over other transducers, capacitive transducer has been used in a variety of applications [44–46]. Also, this type of transducer was used in this work.

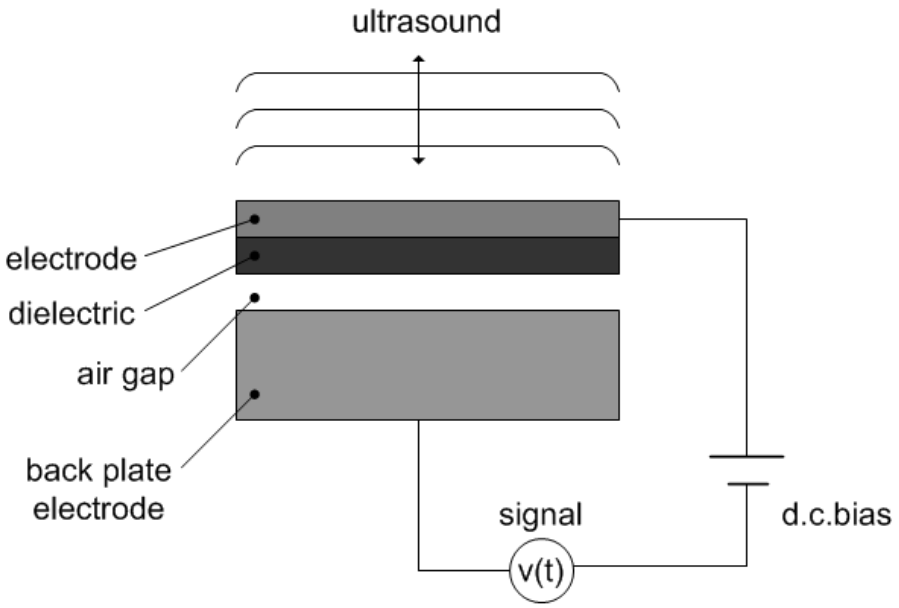

Figure 2.4: The assembly of a signal-element capacitive ultrasound.

2.3.3 Transmitter and Receiver Operation of Capacitive Transducer

Capacitive transducers can be a transmitter, a receiver or both. And the basic principle of operation is electrostatic transduction.

- *Transmitter Operation*: When operating as a transmitter, an alternative current signal is superimposed over the direct current bias to drive the transducer. This alternating voltage produces a corresponding change in charge between the backplate and the membrane, and due to the modulation of the electrostatic force, the

membrane displaces. Then the pockets of air trapped between the two electrodes are compressed, which contributes to the restoring force of the membrane. This pushes the surrounding medium away from the transducer face with the generation of ultrasound that has a frequency corresponding to the frequency of the applied alternative current signal.

- *Receiver Operation*: When operating as a receiver, the membrane displaces when it is subject to an incident ultrasonic wave, and as the separation between the backplate and the membrane changes, a corresponding capacitance change is also produced, which may be detected and amplified using suitable electronic devices. With the availability of microfabrication technologies, capacitive ultrasonic transducers are highly efficient as both transmitters and receivers.

- *Transmit/Receive Switch*: Since the ultrasonic transducer can be applied as both transmitter and receivers, we only used one capacitive transducer. First, the transducer acts as a transmitter. After transmission of the ultrasound, the ultrasonic transducer will switch to receive mode to sense the membrane vibration caused by the returning echoes.

2.4 Principles of Capacitive Transducer

In this section, the principles of capacitive transducer are discussed.

2.4.1 A Capacitor

Generally, a capacitor is a device that is composed of two conducting plates separated by an insulated substance called dielectric, such as air, ceramic, fuel, mica and the like [47]. The electrical charge is stored on the plates, as shown in Figure 2.5. Once the switch is closed, a potential difference voltage V is applied across the two terminals. Then the conducting plate connected with the positive terminal starts to store positive charge and the conducting

plate connected with the negative terminal starts to store negative charge until V matches with the source voltage. The transient response time required to fully charge a capacitor is

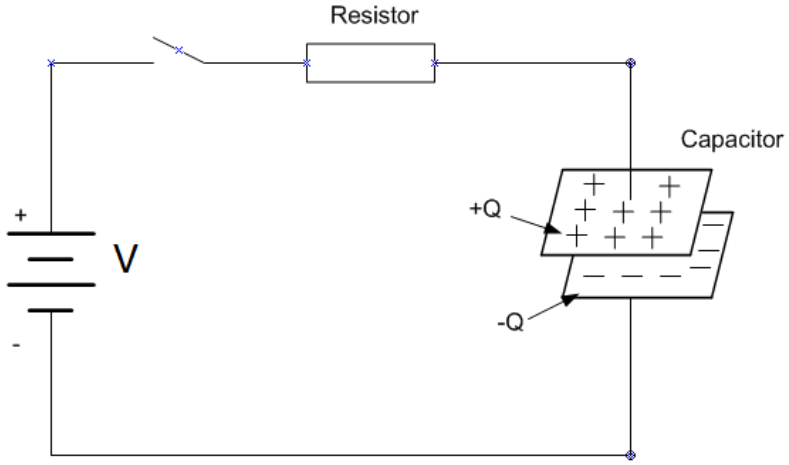

Figure 2.5: Capacitor used in a circuit to store electrical charge.

determined by Time Constant τ, which describes the time it takes to charge a capacitor to 63% of its total capacity [48]. It is defined as in Equation 2.7.

$$\tau = RC \tag{2.7}$$

where R is the value of resistor in Ohms, and C is the capacitance of the capacitor in Farads.

2.4.2 Capacitance

Capacitance, the electrical property of capacitors, is the measurement of the amount of charge that a capacitor can hold at a given voltage applied to the plates [49]. It is measured in Farads and can be calculated as in Equation 2.8.

$$C = \frac{Q}{V} \tag{2.8}$$

where Q is the amount of charge stored on each plate in Coulombs and V is the applied voltage in Volts.

The capacitance only depends on the geometry of the conductors [50]. Generally, the

capacitance value C is determined by the dielectric substance, the distance between the two conducting plates and the area of each plate [51]. The calculation is expressed as shown in Equation 2.9.

$$C = \varepsilon_r \frac{\varepsilon_0 A}{d} \tag{2.9}$$

where ε_r is the relative static permittivity (dielectric constant) of the insulators between the two plates, ε_0 is the permittivity of free space, which is equal to $8.854 \times 10^{-12} F/m$ [52], A is the area of each plate and d is the distance between the two plates.

From the above equation, we can see that a greater separation distance results in lower capacitance value, and the conducting plate with greater surface area is able to store more electrical charge.

2.4.3 Dielectric Constant

The non-conductive material between the two conductive plates has a certain dielectric constant, which is the measure of the material's influence on the electric field. The magnitudes of dielectric constants are different for different materials. For example, the values of dielectric constants for air and gasoline are 1.0 and 2.2 respectively [53].

According to Equation 2.9, it is obvious that the capacitance is proportional to the value of dielectric constant. Then the capacitance can be described simply in terms of the dielectric constant as [52]

$$C = \varepsilon_r C_0 \tag{2.10}$$

where C_0 is the capacitance without dielectric constant.

2.4.4 Capacitive Transducer Applications

A change in position, or properties of the dielectric material of a capacitive sensor is converted into an electrical signal [54]. From Equation 2.9, it can be seen that alteration of any of the four parameters results in a change in the capacitance. Based on this principle, a number of different types of transducers have been developed.

- *Proximity Sensing*: A proximity sensor is a transducer that is used to detect the presence of nearby objects in the absence of any physical contact. The existence of a conducting object near the conducting plate leads to the change of the oscillator frequency, which is detected and sent to the controller unit [55]. The object being sensed is referred to as the proximity sensor's target.

- *Position Sensing*: A position sensor is a device that is able to measure the absolute or relative position of an object [56]. Capacitive type position sensors are normally non-mechanical devices that determine the position based on the physical parameters of the capacitors: area of the conductive plate, dielectric constant and distance between the two plates. They are used in a variety of industrial applications such as fluid level measurement, shaft angle measurement, gear position sensing, digital encoders and counters, and touch screen coordinate systems [53].

Also, there are some capacitive sensors for other applications, such as humidity sensing [57] and tilt sensing [58].

2.5 Image Data Acquisition

For the sake of forming ultrasonic images, the knowledge of ultrasound production, propagation and interactions is required. Each pulse is transmitted and experiences partial reflection from interfaces of two different mediums that create echoes returned to the transducer. Therefore, ultrasound images are created using a pulse-echo mode format of ultrasound production and detection. This approach requires a variety of hardware components including signal generator, transmitter, receiver, amplifier, and display system.

2.5.1 Signal Generator

The signal required to drive the capacitive transducer is a sinusoid burst as shown in Figure 2.6. With the Agilent 33220A 20 MHz Waveform Generator, there are two methods to

produce the burst. The first method is by configuring the function generator to output a waveform with one sinusoid cycle. The rate of the output burst is determined by the internal rate generator or the signal level on the rear-panel *Trig In* connector. The second method is using Matlab to control the function generator by applying the SCPI commands. The burst is generated by setting the following parameters: waveform, mode, frequency, amplitude, burstCount and triggerRate. Then it is downloaded to the function generator. The second method makes it easier to control an arbitrary waveform and it is used in this work.

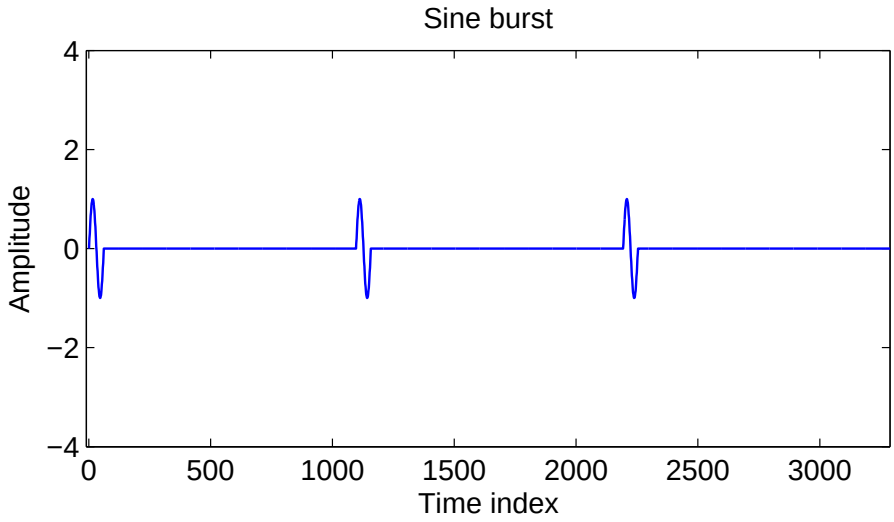

Figure 2.6: Transmitted waveform used.

2.5.2 Pulse-Echo Operation

In the pulse-echo mode of transducer operation, the ultrasound beam is intermittently transmitted, with a majority of time occupied by listening for echoes. The ultrasound pulse is created with a short voltage waveform provided by the pulser of the ultrasound system. The generated pulse is typically two to three cycles long, dependent on the damping characteristics of the transducer elements. With a velocity of sound of 343 m/s, the time delay between the transmission pulse and the detection of the echo is directly related to the

depth of the interface as

$$T = \frac{2D}{c} \tag{2.11}$$

where T is the time, D is the distance and c is the velocity of sound.

2.5.3 Echo Display Methods

The pulse-echo system generates information containing data on the amplitude of the signal. It can be processed in different ways and thereby producing three types of display in the NDT world: A-scan, B-scan and C-scan [59].

- *A-Scan*: A scan is the display of amplitude information from the receiver versus time, and this is the most basic presentation form of ultrasonic waveform data, as shown in Figure 2.7. As echoes return from a boundary between mediums with different acoustic impedance, a digital signal proportional to echo amplitude is formed as a function of time. However, in order to locate the position of the flaws more easily, the X-axis on the A-scan is typically converted into distance. This conversion is accomplished by measuring the velocity of sound in the material that the ultrasonic wave is propagating through.

- *B-Scan*: The B-scan presentations is a profile (cross-sectional) view of the test specimen. In the B-scan, the time-of-flight (travel time) of the sound energy is displayed along the vertical axis and the linear position of the transducer is displayed along the horizontal axis. From the B-scan, the depth of the reflector and its approximate linear dimensions in the scan direction can be determined. The B-scan is typically produced by establishing a trigger gate on the A-scan. Whenever the signal intensity is great enough to trigger the gate, a point is produced on the B-scan. The gate is triggered by the sound reflecting from the backwall of the specimen and by smaller reflectors within the material. It should be noted that a limitation to this display technique is that reflectors may be masked by larger reflectors near the surface [59].

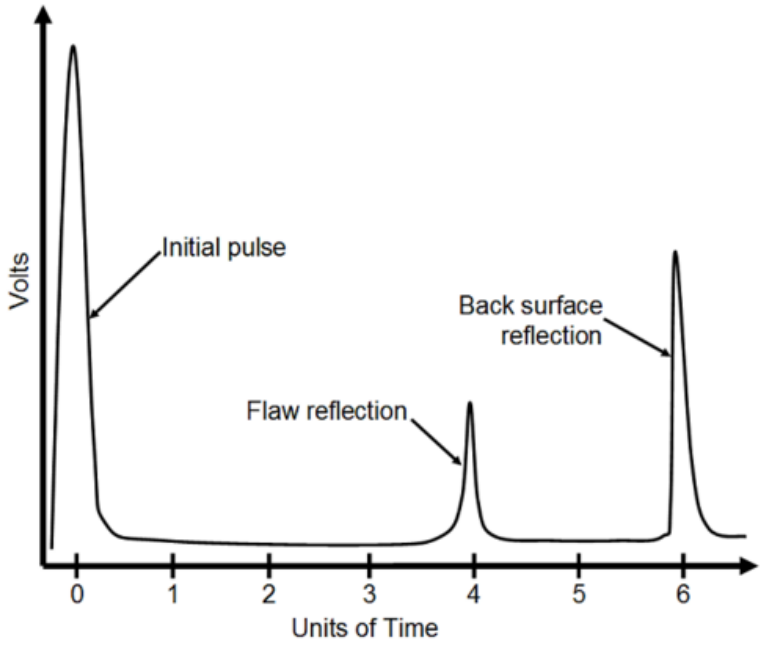

Figure 2.7: A-Scan presentation [59].

- *C-Scan*: In this system the object which is under inspection, is shown as viewed from the top. Normally the depth of the flaw is not indicated. The image is a true-to-scale reproduction of the discontinuity in the job piece and usually a real time image where the formation of the image follows the movement of the probe. The probe movement pattern over the search surface is either closely spaced parallel lines or zigzag or a spiral [60].

Chapter 3

A Non-linear Signal Processing Framework: Higher Order Spectra Analysis

The power spectrum of a time series $x(t)$ describes the distribution of frequency components composing that signal, and it has been a widely used digital signal processing technique in electronic and communication systems. However, there is much more information in a stochastic non-Gaussian or deterministic signal than that is conveyed by its power spectrum. Higher-order spectra which are defined in terms of the higher-order moments or cumulants of a signal, contains this additional information. The Higher-Order Spectral Analysis (HOSA) Toolbox provides comprehensive higher-order spectral analysis capabilities for signal processing applications, and it has been employed in this work. This chapter introduces the basic knowledge of power spectrum and polyspectra, followed by describing higher-order cumulants and the higher-order spectral analysis toolbox. Then the third-order cumulant and fourth-order cumulant were compared, and fourth-order cumulant was found to work better for this application.

3.1 Power Spectrum

Based on Wold's decomposition theorem [61], any discrete-time stationary random process $x(n)$ can be expressed as:

$$x(n) = y(n) + z(n) \tag{3.1}$$

where $y(n)$ and $z(n)$ are processes uncorrelated with each other. $y(n)$ has a causal linear process representation

$$y(n) = \sum_{k=0}^{\infty} h(k)u(n-k) \tag{3.2}$$

where $h(0) = 1, \sum_{k=0}^{\infty} h^2(k) < \infty$, and $u(n)$ is a white-noise process. $z(n)$ is a predictable process orthogonal to $y(n)$ with zero variance. The autocorrelation of a stationary process $x(n)$ is defined by,

$$R_{xx}(m) = E\{x^*(n)x(n+m)\} \tag{3.3}$$

From Wiener-Khintchine theorem [62], the power spectrum function is defined as the Fourier Transform of the autocorrelation sequence

$$P_{xx}(f) = \sum_{k=-\infty}^{\infty} R_{xx}(k)e^{-i2\pi fk} \tag{3.4}$$

Another equivalent definition of power sepctrum is given by

$$P_{xx}(f) = E\{X(f)X^*(f)\} \tag{3.5}$$

where $X(f)$ is the Fourier Transform of $x(n)$

$$X(f) = \sum_{-\infty}^{\infty} x(n)e^{-j2\pi fn)} \tag{3.6}$$

As we can see from Equation 3.4, the power spectrum only exists provided that the autocorrelation sequence is absolutely summable. Also, the power spectrum is real valued and nonnegative. It is a second-order moment or cumulant spectra and is sufficient for the statistical description of a Gaussian process of known mean. However, in some practical situations, we have to go beyond the power spectrum domain to obtain more

information, which could be gained from higher-order (greater than 2) spectra, also known as polyspectra.

3.2 Polyspectra

Polyspectra comprises higher-order moment spectra and higher-order cumulant spectra. Third-order spectra is called the bispectrum and fourth-order spectra is called trispectrum. Higher-order moments are natural generalizations of the autocorrelation, and cumulants are specific nonlinear combinations of the moments. As illustrated in Figure 3.1, the two categories benefit different from different types of signals [63]. Compared with second-

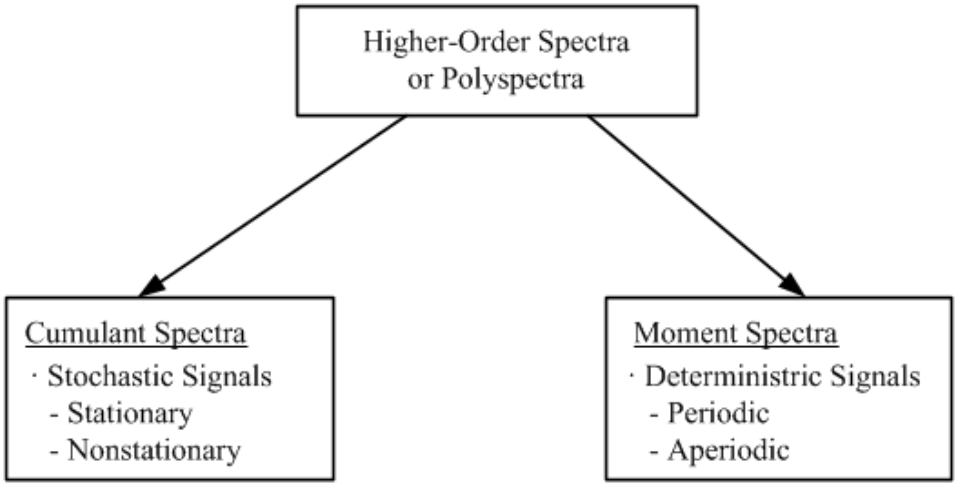

Figure 3.1: The polyspectra classification map.

order spectra, polyspectra is advantageous in three aspects. The first aspect is that all higher-order cumulant spectra of a Gaussian process is zero. With this feature, the additive Gaussian noise present in a deterministic signal can be eliminated by transforming to a higher-order cumulant domain. Therefore, cumulant spectra domains maintain high signal-to-noise ratio (SNR) in many applications. The second aspect is that polyspectra keeps the true phase property of signals. The autocorrelation or power spectrum domain suppresses phase information, which can only be reconstructed accurately if the signal is minimum phase. However, because of polyspectra's ability for preserving both magnitude

and nonminimum phase information, reconstruction of nonminimum phase signal can be achieved as well in higher-order spectrum domains. The third aspect is based on the fact that it is quite natural to analyze the nonlinearity of a system operating under a random input by using higher-order spectra [63]. For the two types of higher-order spectra, cumulants spectra is more useful in the processing of random signals [63].

3.3 High-order Cumulants

3.3.1 Definition of kth-order Cumulant and Polyspectra

The first-order cumulant for a stationary process is equal to the mean, $C_{1x} = E\{x(t)\}$. In order to define higher-order cumulants, it is more convenient to assume that the mean is zero. For a process with nonzero mean, the mean could be subtracted. Then the second-, third-, and fourth-order auto-cumulants are defined as [64]

$$C_{2x}(k) = E\{x^*(n)x(n+k)\} \tag{3.7}$$

$$C_{3x}(k,l) = E\{x^*(n)x(n+k)x(n+l)\} \tag{3.8}$$

$$\begin{aligned} C_{4x}(k,l,m) &= E\{x^*(n)x(n+k)X(n+l)x(n+m)\} \\ &= -C_{2x}(k)C_{2x}(l-m) - C_{2x}(k-m) \\ &= -M^*_{2x}(m) - M_{2x}(k-l) \end{aligned} \tag{3.9}$$

where $M_{2x} = E\{x(n)x(n+m)\}$, which is the second-order moment and equals to $C_{2x}(m)$.

The kth-order polyspectrum is defined as the Fourier transform of the corresponding cumulant sequence:

$$S_{2x}(f) = \sum_{k=-\infty}^{\infty} C_{2x}(k)e^{-j2\pi fk} \tag{3.10}$$

$$S_{3x}(f_1, f_2) = \sum_{k,m=-\infty}^{\infty} C_{3x}(k,l)e^{-j2\pi(f_1k+f_2l)} \tag{3.11}$$

$$S_{4x}(f_1, f_2, f_3) = \sum_{k,l,m=-\infty}^{\infty} C_{4x}(k, l, m) e^{-j2\pi(f_1 k + f_2 l + f_3 m)} \tag{3.12}$$

The definition of cross-cumulants is similar to cross-correlation. For example, the third-order cross-cumulants and cross-bispectrum are defined as Equation 3.13 and Equation 3.14 respectively.

$$C_{xyz}(k, l) = E\{x^*(n) y(n + k) z(n + l)\} \tag{3.13}$$

$$S_{xyz}(f_1, f_2) = \sum_{k,l=-\infty}^{\infty} C_{xyz}(k, l) e^{-j2\pi(f_1 k + f_2 l)} \tag{3.14}$$

3.3.2 Bias, Variance and MSE of an Estimator

Let $x(n)$ denote a stationary process with the assumption that all relevant statistics exist having finite values. Let θ denote some statistic. To estimate it, we use an estimator which is a function based on N observations $\hat{\theta}_N\{x(1), x(x), ..., x(N)\}$. Clearly, $\hat{\theta}_N$ is not equal to θ. The bias of $\hat{\theta}_N$ is defined as $Bias(\hat{\theta}_N) = E(\hat{\theta}_N) - \theta$. If it is 0, the estimator $\hat{\theta}_N$ is said to be unbiased.

However, besides the bias, there is another parameter mean square error (MSE) that is more important for characterizing the estimator. The MSE of an estimator is $E((\hat{\theta}_N - \theta)^2)$, which can be expressed as the following equation,

$$\begin{aligned} E((\hat{\theta}_N - \theta)^2) &= E(\hat{\theta}_N^2 + \theta^2 - 2\hat{\theta}_N\theta) = E(\hat{\theta}_N^2) + \theta^2 - 2\theta E(\hat{\theta}_N) \\ &= E(\hat{\theta}_N^2) - E^2(\hat{\theta}_N) + E^2(\hat{\theta}_N) - 2\theta E(\hat{\theta}_N) + \theta^2 \\ &= Var(\hat{\theta}_N) + Bias^2(\hat{\theta}_N) \end{aligned} \tag{3.15}$$

It can be seen from Equation 3.15 that MSE is composed of a sum of the variance and bias of the estimator. Both quantities need to be taken into account for achieving good estimation performance.

3.3.3 Estimating Cumulants and Polyspectra

In practical situations, $x(n)$ is a finite amount of data with length N, and the sample estimates of cross-cumulants are given by

$$\hat{C}_{xy}(k) = \frac{1}{N_3} \sum_{n=N_1}^{N_2} x^*(n)y(n+k) \tag{3.16}$$

$$\hat{C}_{xyz}(k,l) = \frac{1}{N_3} \sum_{n=N_1}^{N_2} x^*(n)y(n+k)z(n+l) \tag{3.17}$$

$$\begin{aligned} \hat{C}_{wxyz}(k,l,m) &= \frac{1}{N_3} \sum_{n=N_1}^{N_2} w^*(n)x(n+k)y(n+l)z^*(n+m) \\ &= -\hat{C}_{wx}(k)C_{yz}(l-m)) - \hat{C}_{wy}(l)C_{xz}(k-m) \\ &= \hat{M}^*_{wz}(m)\hat{M}_{xy}(l-k) \end{aligned} \tag{3.18}$$

where $\hat{M}_{xy}(l-k)$ equals to

$$\hat{M}_{xy}(l-k) = \frac{1}{N_3} \sum_{n=N_1}^{N_2} x(n)y(n+l-k) \tag{3.19}$$

N_1 and N_2 are specified so as to constrain the number of samples involved in the summations to be N. Take the third-order cumulant for example, if N_3 is set to the actual number of the summation terms N, then the unbiased estimate is obtained such that

$$E\{\hat{C}^N_{xyz}(k,l)\} = C_{xyz}(k,l) \tag{3.20}$$

Estimates of autocomulants are obtained when $w = x = y = z$. These estimates are said to be consistent if the stationary processes $x(n), y(n), z(n)$ satisfies some weak condition [65]. When N is large enough, the sample variance of third-order cross-cumulant is given by

$$var\{\hat{C}^N_{xyz}(k,l)\} = c/N \tag{3.21}$$

where c is a finite constant depending on the cross-cumulants of orders of the processes $x(n), y(n), z(n)$. All the definitions are under the assumption that the means of the

processes are zero. So, the sample mean is subtracted before calculation.

The estimator of the power spectrum is the Fourier transform of $\hat{R}_{xx}^N(m)$, which is the estimate of auto-correlation,

$$I_{xx}^N = \sum_{m=-N-1}^{N-1} \hat{R}_{xx}^N e^{-j2\pi fm} = \frac{1}{N} \left| \sum_{k=0}^{N-1} x(k) e^{-j2\pi fk} \right|^2 \tag{3.22}$$

Since $E\{\hat{R}_{xx}^N(m)\} = R_{xx}(m)$, $I_{xx}^N(f)$ is an unbiased estimator of $P_{xx}(f)$. However, as $var(P_{xx}^N(f)) = P_{xx}^2(f)$, which means that its variance does not go to zero as $N \to \infty$, $I_{xx}^N(f)$ is not a consistent estimator [66].

The estimate of the cross-bispectrum is the Fourier transform of the third-order cumulant sequence, which is,

$$\begin{aligned} I_{xyz}^N(f) &= \sum_{k=-N-1}^{N-1} \sum_{I=-N-1}^{N-1} \hat{C}_{xyz}(k,l) e^{-j2\pi f_1 k} e^{-j2\pi f_2 l} \\ &= \frac{1}{N^2} X_N^*(f_1 + f_2) Y_N(f_1) Z_N(f_2) \end{aligned} \tag{3.23}$$

where $X_N(f)$ is the Fourier transform of $\{x(n)\}_{n=0}^{N-1}$.

3.4 Higher Order Spectral Analysis Toolbox

The HOSA toolbox is a collection of M-files that implement a variety of advanced signal processing algorithms including estimation of auto- and cross-cumulants, spectra and polyspectra, and computation of time-frequency distributions. Also, algorithms for testing of Gaussianity and Linearity of a time series are available.

In this toolbox, the functions $cum2x$, $cum3x$, and $cum4x$ are used to estimate cross-cumulants of orders 2, 3, and 4 respectively. Function $cumest$ is used to estimate the autocumulants. Hence, the sample estimates of cumulants using the overlapped-segment methods is computed as

$$cvec = cumest(y, norder, maxlag, samp_seg, overlap, flag, k1, k2)$$

where $cvec$ is the result of sample estimates of cumulants, y is data matrix, $maxlag$ defines the maximum lag of the comulants to be computed and the default value is 0, $samp\_seg$ specifies the number of samples of each segment and the default value is the length of y, $overlap$ the percentage of overlap between segments with default value 0 and maximum allowed value 99, $flag$ decides whether biased or unbiased estimates are computed.

Bispectrum estimation can be obtained using the indirect method $bispeci$ and direct method $bispecd$ as follows,

$$[bspec, waxis] = bispeci(y, nlag, samp\_seg, overlap, flag, nfft, wind)$$

$$[bspec, waxis] = bispecd(y, nfft, wind, samp\_seg, overlap)$$

where y is the data matrix being processed, $nlag$ specifies the number of cumulant lags to be computed, $samp\_seg$ indicates the number of samples per segment, $overlap$ specifies the percentage of overlap between segments, $flag$ is either biased or unbiased, $nfft$ describes the FFT length and $wind$ specifies the lag-domain smoothing window.

3.5 Analysis of Ultrasound Scans Based on Higher Order Cumulants

As indicated by Nikias and Mendel [63], the power spectrum does not offer information about the phase relations between frequency components as the information depends on the autocorrelations of the signals but higher order spectral analysis contains such information. With the method of higher order spectra and phase matching estimate, not only the Gaussian noise but also the non-Gaussian can be removed [67, 68]. Therefore, it is widely applied to image processing, signal denoising and pattern recognition fields. Also, higher order spectral analysis has been introduced as an attractive tool to denoise ultrasound images not only in the medical area but also in the industrial area [69–71].

In recent years polyspectra has been proposed to extract features from acoustic sounds

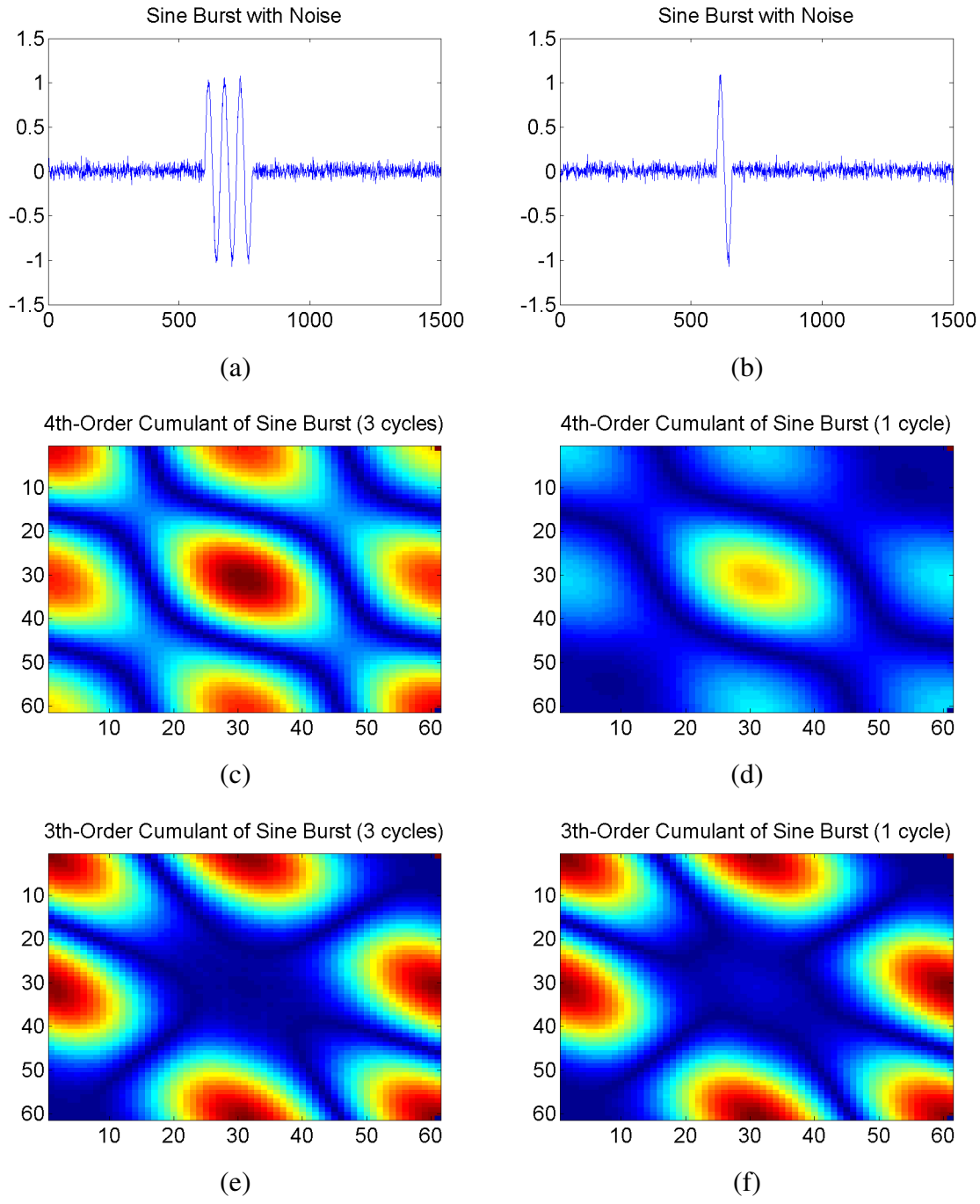

Figure 3.2: (a) Sine burst (3 cycles) with Gaussian noise added, (b) Sine burst (1 cycle) with Gaussian noise added, (c) Fourth-order cumulants of the signal in (a), peak = -33.07 db, (d) Fourth-order cumulants of the signal in (b), peak = -36.2496 db, (e) Third-order cumulants of the signal in (a), peak = -39.25 db,(f) Third-order cumulants of the signal in (b), peak = -39.41 db.

for non-destructive evaluation [72]. As mentioned in [68], higher-order spectra can be a powerful signal processing tool for detecting a non-Gaussian or transient signal in Gaussian

or non-Gaussian noise. It is based on work reported in [68] and [72] that we were motivated to use the HOS in the analysis of the ultrasound scans looking for a reliable fault detection test. As shown in Figure 3.2, the simulations were conducted on sinusoid bursts with three cycles and one cycle respectively, and Gaussian noise with expectation 0.05 and variance 0.01 was added. Figure 3.2 (c) and (d) are the results for fourth-order cumulants, and the peak in (c) is approximately 3 db higher than the peak in (d). Figure 3.2 (e) and (f) are the results for three-order cumulants, and the peaks are almost the same. Therefore, fourth-order cumulants was chosen for this work.

Chapter 4

Fault Detection on Power Cables Based on Ultrasound Images and Higher Order Spectra

In this chapter, a new method of fault detection on XLPE power cables based on ultrasound images and fourth-cumulant is described. The transmitted signal for activating the transducer was generated by Matlab and downloaded to the function generator. Forty-eight scans were obtained by rotating the cable 360 degrees. The first highest point of the received signal was considered to be the surface of the cable. The peaks of the samples within XLPE were compared and a threshold was set to detect the faults. In addition, higher order spectral analysis was introduced to decide if there was a fault in the cable.

4.1 Instrumentation Setup

A series of experiments were set up using an Agilent 33220A 20 MHz Function/Arbitrary Waveform Generator for sending transmitted signal generated by Matlab, a Tektronix MDO3000 Oscilloscope for data acquisition, a commercial ultrasound system from VN Instruments using an air transducer operating around a frequency of 802.8 KHz as shown

in Figure 4.1.

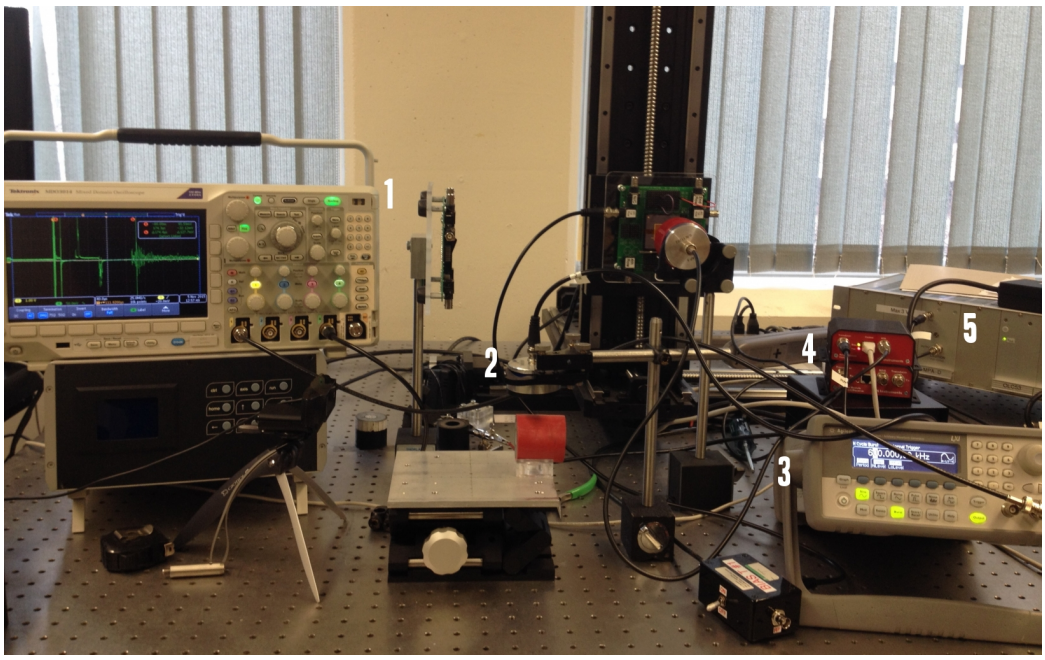

Figure 4.1: Ultrasound equipment set up used in this work (1 oscilloscope, 2 ultrasonic transducer, 3 function generator, 4 remote module and hub unit, 5 power amplifier.)

4.1.1 Introduction of the Instruments

The Agilent 33220A function/arbitrary waveform generator uses direct digital synthesis (DDS) techniques to create a stable, accurate output signal. Also, waveforms can be created and downloaded by using Matlab instrument control toolbox, which is the way used to generate transmitted signal in this work. The Tektronix MDO3000 oscilloscope is a 6-in-1 integrated oscilloscope that includes an integrated spectrum analyzer, arbitrary function generator, logic analyzer, protocol analyzer and digital voltmeter/counter. It is completely customizable and fully upgradeable.

The power amplifier, control hub, remote module unit and ultrasonic transducer are provided by VN Instruments Ltd.

- *Power Amplifier*: The power amplifier has a simple analog input that uses a Lemo style connector. Input signals should be limited to +/-3V. A lemo to BNC adaptor is

(a) (b)

Figure 4.2: (a) Function generator. (b) Oscilloscope.

(a) (b) (c) (d)

Figure 4.3: (a) Power amplifier. (b) Remote module unit. (c) Control hub. (d) Transducer.

provided to facilitate connecting signal sources to the amplifier. The power output from the amplifier should be connected directly to the MPA input on the remote module.

- *Remote Module*: VN Instruments Ltd. provides two different remote module units. One is setup to do pulse echo measurements. This unit has a single transducer connection. Any power signal provided to the MPA port is sent to the transducer. Any signal received by the transducer is sent to the control hub. The second remote unit has two transducer connections. One transducer is the transmitter, the other one is the receiver. Signals provided to the MPA port are sent to the Tx transducer. Any signals received on the Rx transducer are amplified and sent to the Hub where they can be read using a digitizer. The first remote module type unit was used in this work.

- *Control Hub*: The control hub is used to power the remote modules, to control the gain of the remote modules and to activate and deactivate the HV bias supply contained within the remote module itself. The hub also splits the amplified signals

taken from the remote module and puts the signals onto a BNC connector. The hub has four RJ45 connectors and four matching BNC connectors. The hub can power and operate up to four remote modules at the same time. All four remote modules will have the same gain setting.

- *Transducer*: The capacitive transducers developed by VN Instruments Ltd. are well suited to industrial and research environments because of their superior bandwidth, great sensitivity and stability over time. They function well under various conditions, can be cleaned with conventional solvents and are suitable for all air coupled applications. The transducers require a stable and quiet high voltage bias source, which can be provided by VN's remote modules under full software control of the SIA-7 [20]. For this work, CAP5 transducer operating around a frequency of 802.8 KHz was used as shown in Figure 4.4.

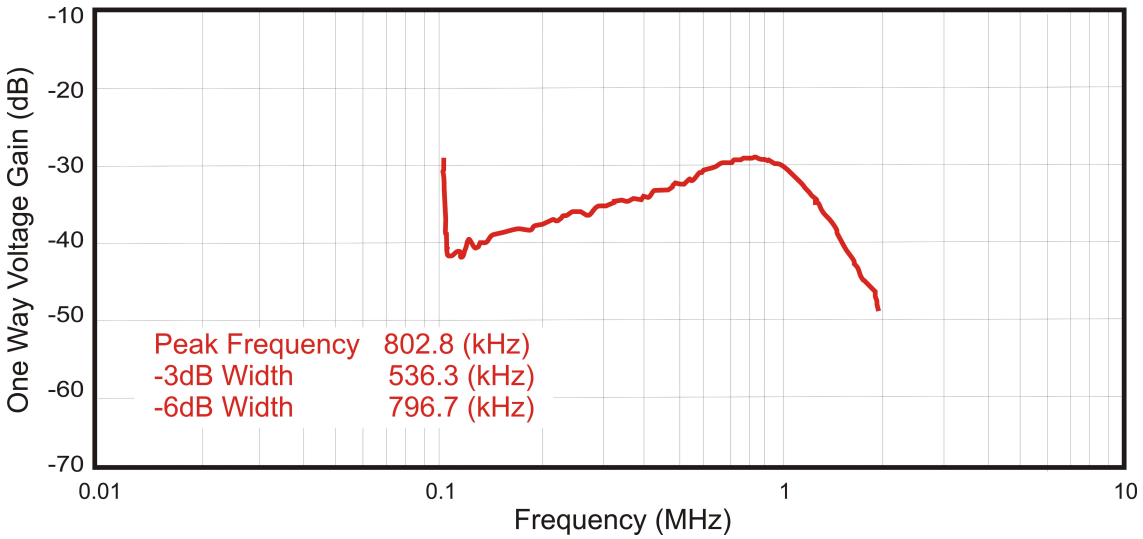

Figure 4.4: Ultrasound transducer characterization.

4.1.2 System Setup

Firstly, the DC power supply is connected to the hub unit. The front side of the hub has a small LCD display that shows the current gain setting as well as small buttons used to increase or decrease the gain and another button that is used to turn the HV bias on or off.

Secondly, an RJ45 patch cable (CAT 5) is attached between the hub and the remote module. Then the BNC connector directly below the RJ45 patch is connected to the oscilloscope. Also, one BNC cable is required to connect the CAP 5 transducer with the remote module and another BNC cable is needed between the power output from the amplifier and the MPA input on the remote module. The next step is to connect a signal source from function generator to the amplifier. Lastly, the oscilloscope and function generator are connected to the computer via a usb cable.

4.2 Test the System

Before data collection, some tests have been implemented to prove the feasibility of the system. The first test was on a black XLPE cable with the conductive center of the cable being removed, and then a foreign object, a metal cylinder, was introduced at the center of the cable. As it can be seen in Figure 4.5, the received waveforms differ considerably in amplitude as the return when the object is introduced, part (b), has higher amplitudes due to the immediate response from this object and no further attenuation in air is experienced as the waveforms travel a longer distance as shown in part (a).

Another test consisted on comparing the two received scans, one of which was collected when there was a red XLPE cable right under the transducer, and the other that was collected when there was no cable. From the results in Figure 4.6, we can see that the amplitude in part (a) around time index 2200 is much higher, because the transmitted signal reached the surface of the cable and then bounced back. And based on the theory, the first highest peak of the received scan indicates the cable surface. As we can see from Figure 4.7, the time difference between the transmitted signal and the peak of received signal is 174 μs. Since the speed of sound in air at 20 degrees centigrade is 343 m/s [41], the distance between the transducer and the cable can be calculated by $0.343 \times 174 \ / \ 2 = 30 \ mm$, which matches the measurement in Figure 4.7.

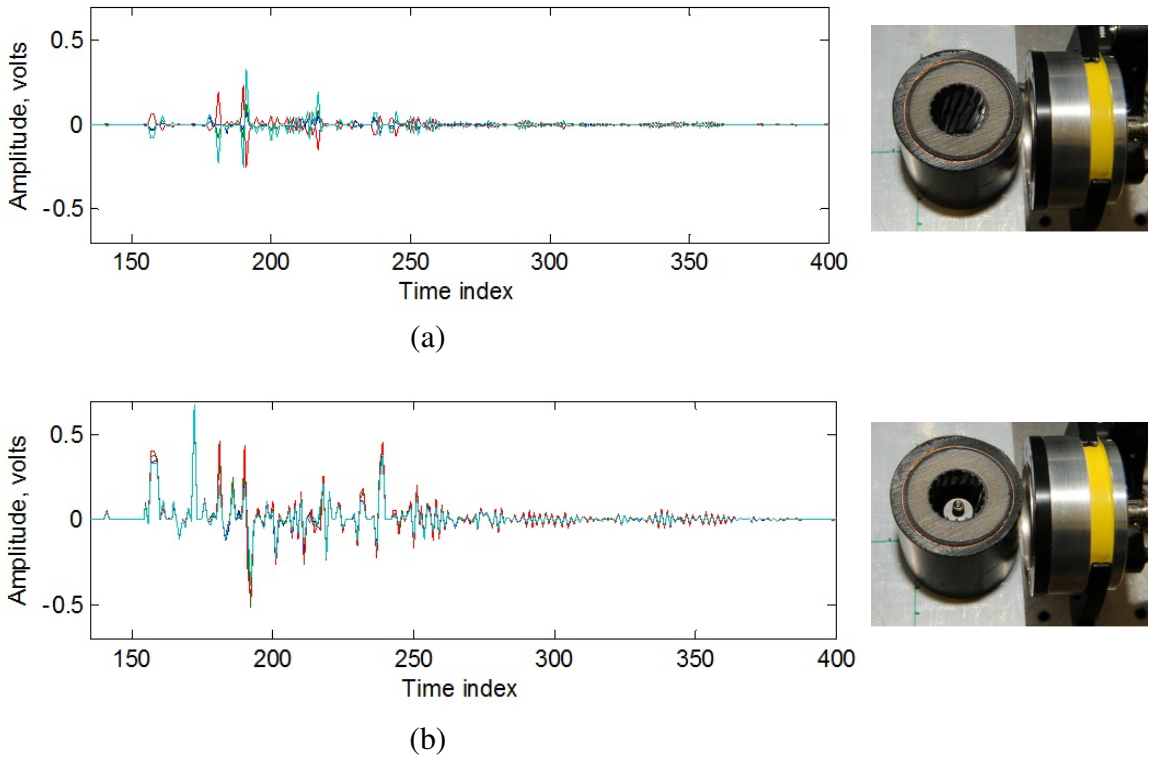

Figure 4.5: (a) Two examples of data collected with no foreign object at the center of the cable. (b) Another two examples when a metal cylinder was placed at the center. Note the difference on waveforms received for the two different cases.

4.3 Data Collection

In this section, the process of data collection is discussed in detail. The transmitted signal generated by Matlab was sent to the function generator and then Matlab read the data from the oscilloscope.

4.3.1 Generate the Transmitted Signal

The transmitted burst signal was generated by Matlab R2014a and then sent to the function generator. In order to communicate Matlab with the instruments, we installed the Virtual Instrument Standard Architecture (VISA) software, which is a standard defined by Agilent Technologies and National Instruments for communicating with instruments regardless of the interface. The instrument Control Toolbox was also installed to enable Matlab connect to instruments via VISA so that we could send data to the function generator

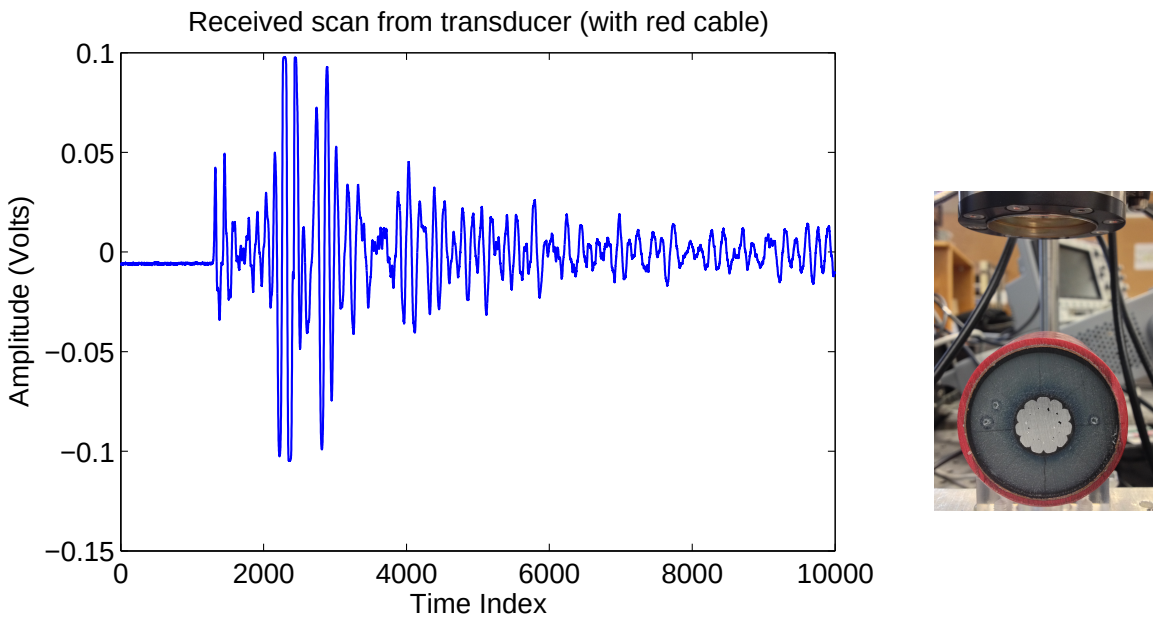

(a)

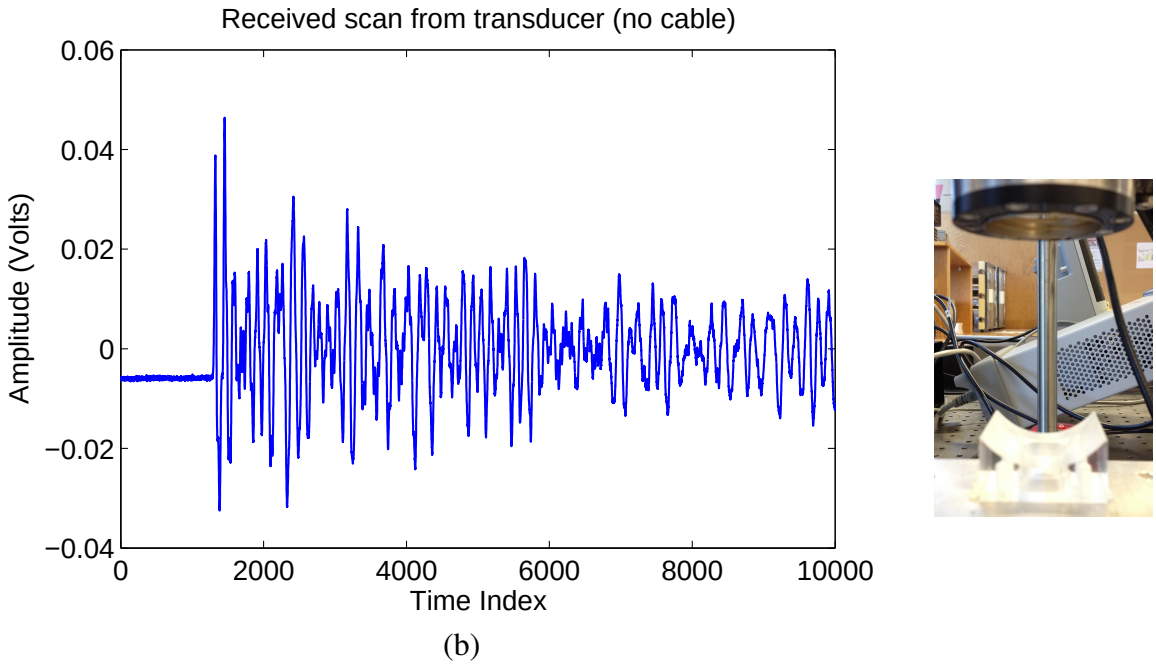

(b)

Figure 4.6: (a) Two examples of data collected with a red cable beneath the transducer. (b) Another two examples when there is no cable under the transducer. Note the difference on waveforms received for the two different cases.

and read data from the oscilloscope for analysis and visualization. The instruction *instrhwinfo('ivi')* was for checking that all the software had been installed correctly. Then we created an oscilloscope instance by *myScope = oscilloscope()*, set the resource which

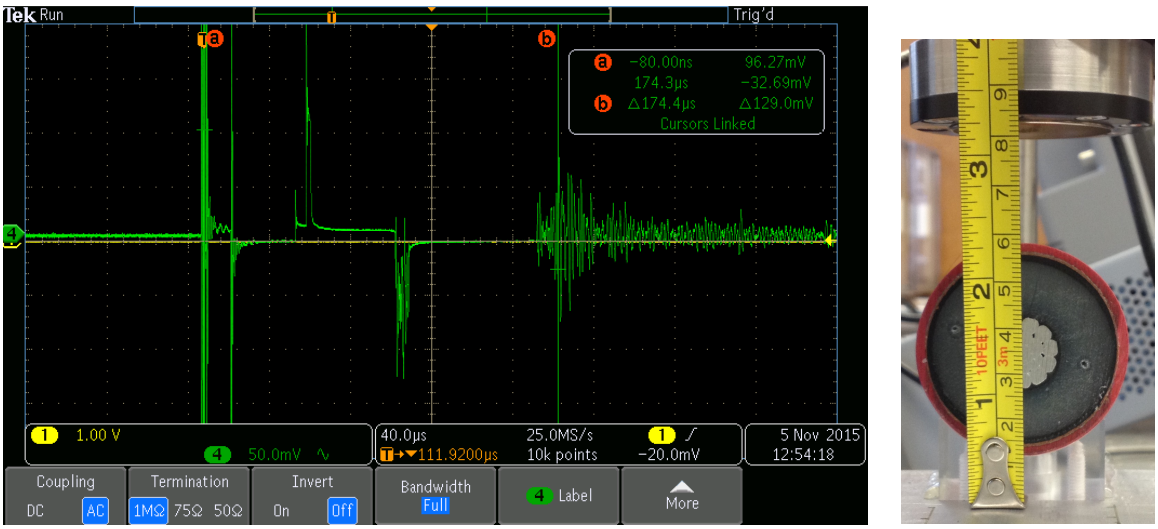

Figure 4.7: (a) The time difference between the transmitted signal and the first highest peak of the received scan. (b) The distance between the transducer and the surface of the red cable.

specially identify the oscilloscope, and connected it by *connect(myScope)*. Same steps were implemented for connecting to the function generator. After that, we set the parameters to configure the waveform to be a continuous burst with one sinusoid cycle, as shown in Figure 4.8. Lastly, we enabled the output using the *enableOutput* function.

Algorithm 1 Generate the transmitted signal

```
instrhwinfo ('ivi');
myScope = oscilloscope();
set(myScope, 'Resource', ' USB::0x0699::0x0408::C012063::INSTR');
connect(myScope);
myFGen = fgen();
myFGen.Resource = 'USB::0x0957::0x0407::MY44061223::INSTR';
connect(myFGen)
selectChannel(myFGen, '1');
set(myFGen, 'Waveform', 'sine');
set(myFGen, 'Mode', 'Burst');
f = 600000;
set(myFGen, 'Frequency', f);
set(myFGen, 'Amplitude', 1.5);
set(myFGen, 'BurstCount', 1);
TR = 1000*(1/f);
set(myFGen, 'TriggerRate', TR);
enableOutput(myFGen);
```

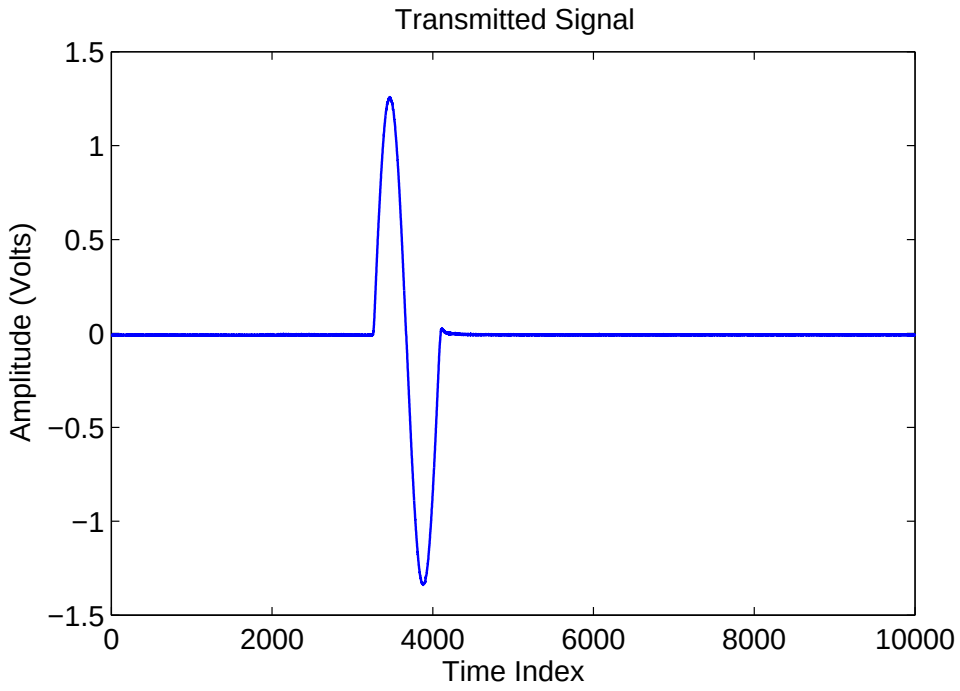

Figure 4.8: Transmitted signal.

4.3.2 Collect Received Scans from Transducer

Two sample cables used in this work are shown in Figure 4.9. The first one is a good cable and the second one is a bad cable with three small holes.

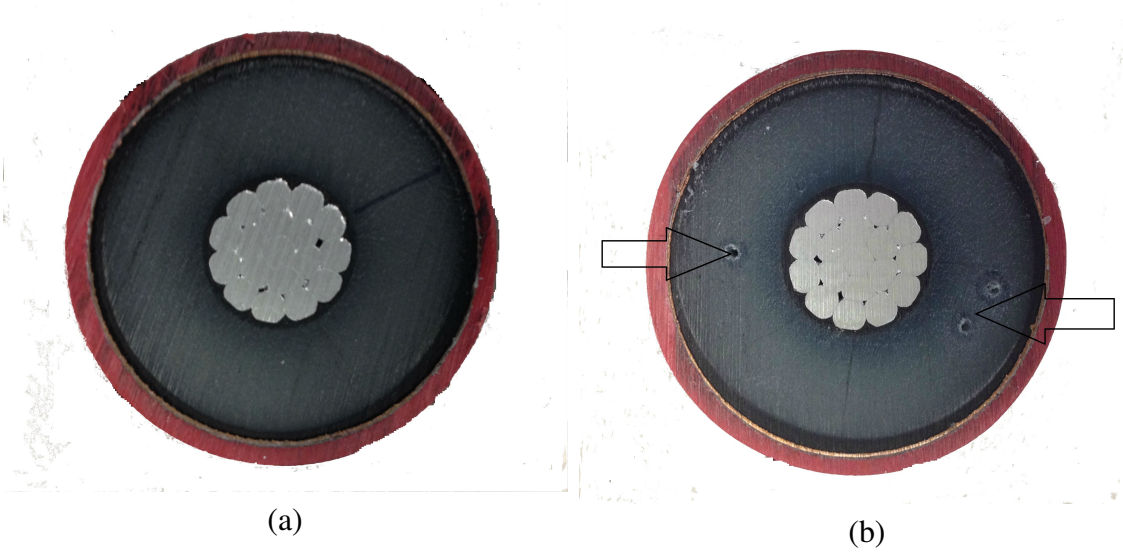

Figure 4.9: Picture of cables under test. (a) Good cable. (b) Bad cable.

The Tektronix OpenChoice Desktop application can be used to capture the oscilloscope screen images, waveform data and settings from a Microsoft Windows computer as shown in Figure 4.10. It saves all the information including record length, sample interval, trigger point, time index, amplitude and so on. However, besides saving the samples interval and time information once for all the scans, we just need the amplitude information. In addition, clicking on the ”Get Data” and ”Save As” buttons for each position makes it time consuming. Thus, we use the code in Algorithm 2 to save data automatically.

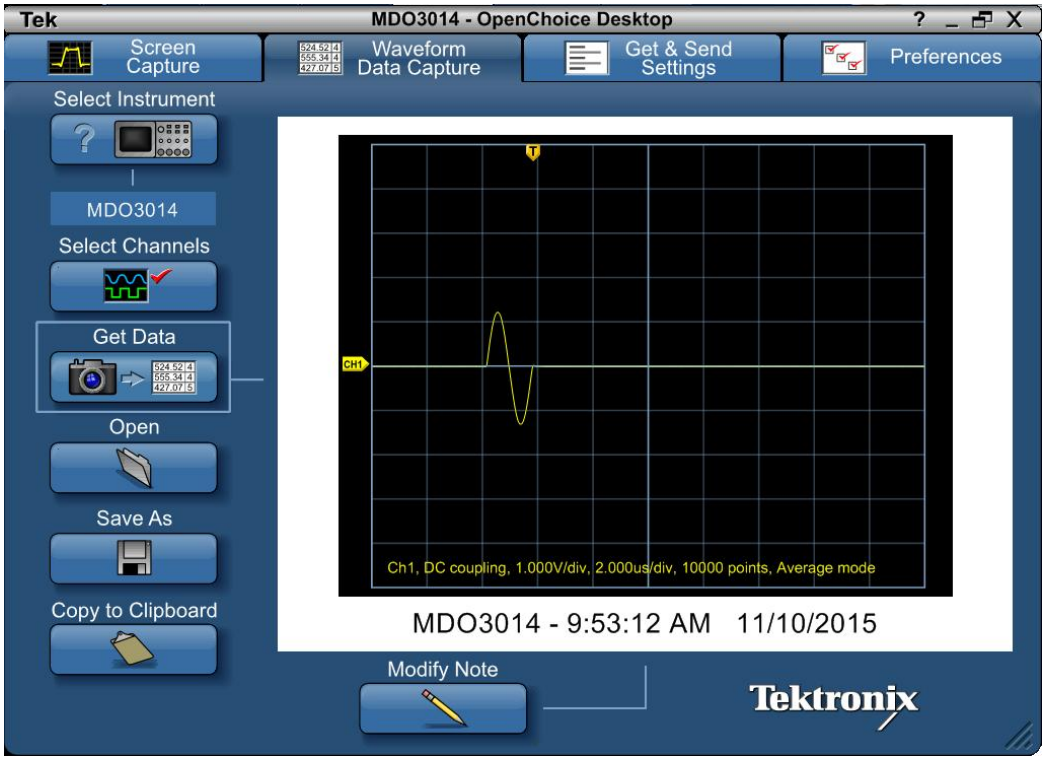

Figure 4.10: OpenChoice Desktop.

A Logitech HD Pro Webcam C920 was place in front of the cable for image acquisition, as shown in Figure 4.11. A the code in Algorithm 2 enables Matlab to capture the computer screen so that the image at each cable position can be saved.

Algorithm 2 Acquire received scans and capture images

```
K = 1;
number = 1001;
while K == 1; do
    K = menu('Choose','More','Stop');
    close all
    w = getWaveform(myScope);
    dataName = ['data',num2str(number),'.csv'];
    csvwrite(dataName,w);
    robo = java.awt.Robot;
    target=java.awt.Rectangle(x,y,w1,h);
    image = robo.createScreenCapture(target);
    rasta = image.getRGB(0,0,w1,h,[],0,w1);
    rasta = 256^3+rasta;
    B = uint8(mod(rasta,256));
    G = uint8(mod((rasta-int32(B))./256,256));
    R = uint8(mod((rasta-256*int32(G))./65536,256));
    X.cdata = uint8(zeros(h,w1,3));
    X.cdata(:,:,1) = reshape(R,[w1 h])';
    X.cdata(:,:,2) = reshape(G,[w1 h])';
    X.cdata(:,:,3) = reshape(B,[w1 h])';
    X.colormap = [];
    imagen = X.cdata;
    imag2 = imagen(80+180:420+180,1:350,:);
    imageName = ['image',num2str(number),'.jpg'];
    number = number +1;
    imwrite(imag2,imageName)
end while
```

4.4 Results

In this section, we analyzed all the collected scans on the good cable and faulty cable to verify that the faults on the XLPE power cables could be detected based on ultrasound scans and fourth-order cumulants.

4.4.1 The Results Based on Ultrasond Image

Figure 4.12 compares the difference of two received scans, one of which was collected when there was no cable lying below the transducer and the other one of which was collected when there was a red faulty XLPE cable under the transducer.

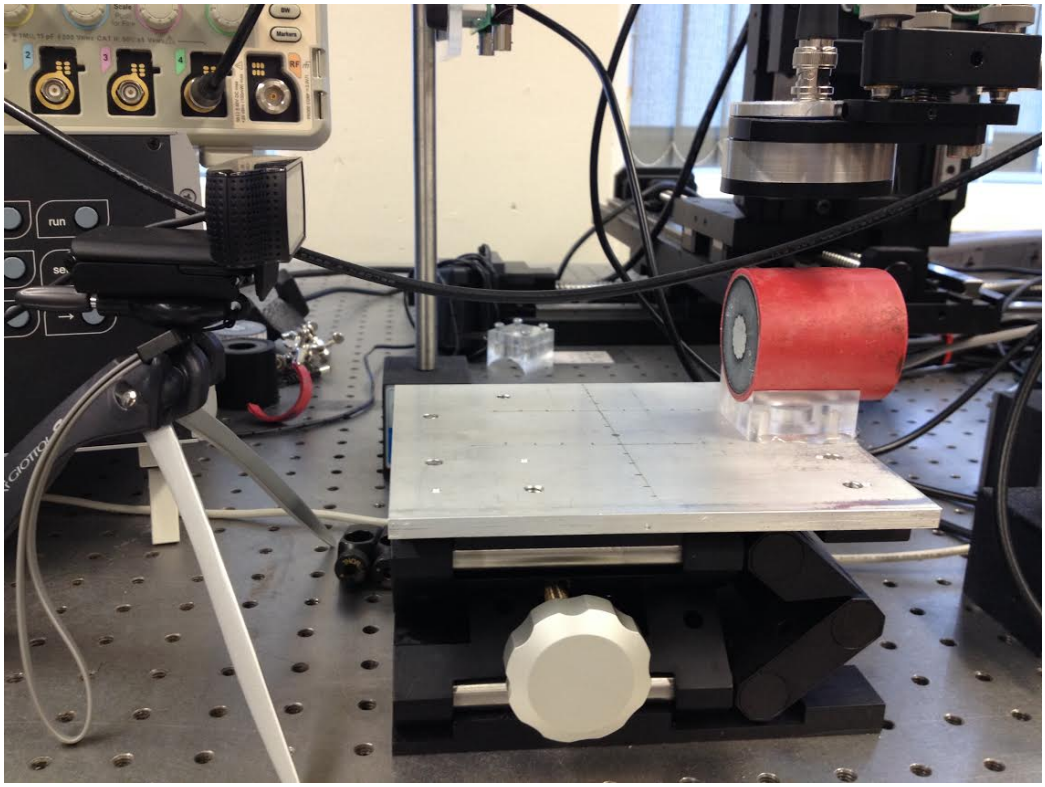

Figure 4.11: Logitech webcam for image acquisition.

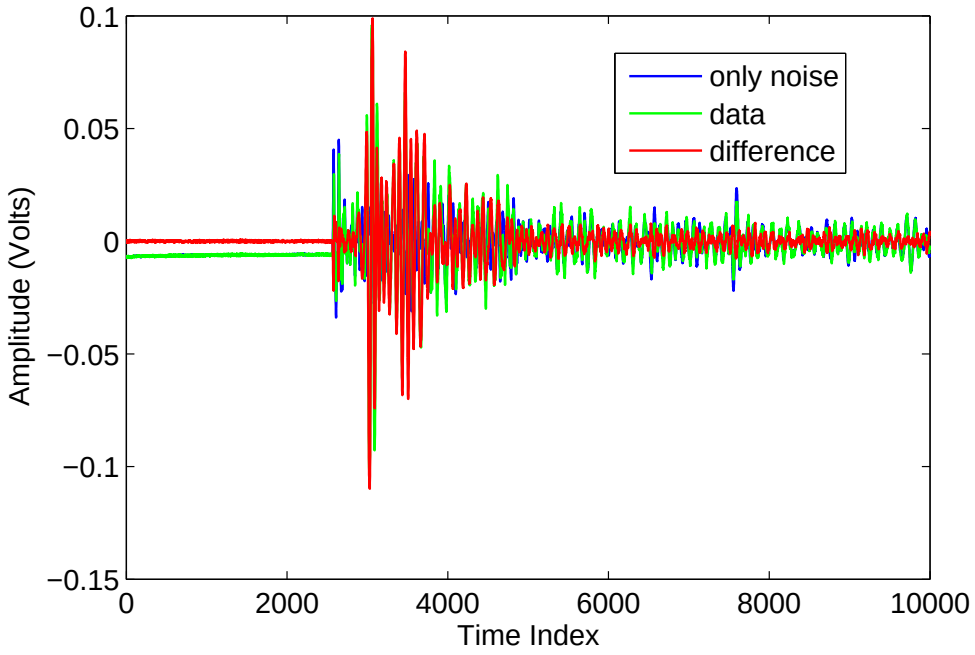

Figure 4.12: The difference between the two received scans when there is cable and no cable.

As we have discussed before, the first highest point of the received scan indicate the surface of the cable. Also, based on the propagation sound velocity in air and the distance between the transducer and the cable, we were able to find the approximate position of the sample corresponding to the surface. Therefore, we just focused on the area around that point and found the positions which have the maximum absolute values as indicated by the black circles shown in Figure 4.13. It is not a straight line due to the bumps on the surface of the cable. We also needed to calculate the propagation sound velocities of the materials so that the received signals only within the XLPE material were analyzed. Figure 4.14 shows the dimensions and velocities obtained using a Krautkramer USN58 ultrasound system. Also shown in the picture are the three faults in the cable that were introduced by drilling holes of approximately 4 mm. The arrows indicate not only the position of these holes but also the distance between these holes and the surface to the XLPE layer.

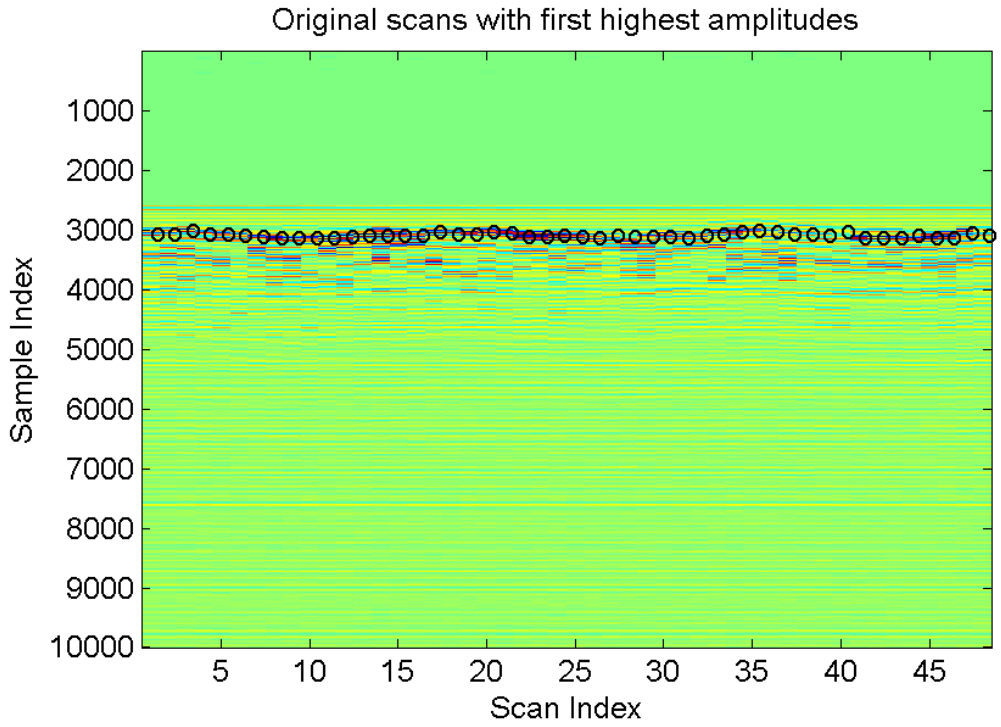

Figure 4.13: Original scans with first highest amplitudes.

From the data saved using the OpenChoice Desktop application, we knew that the sample interval was $2 \times 10^{-8}s$. Therefore, the numbers of samples within the outer

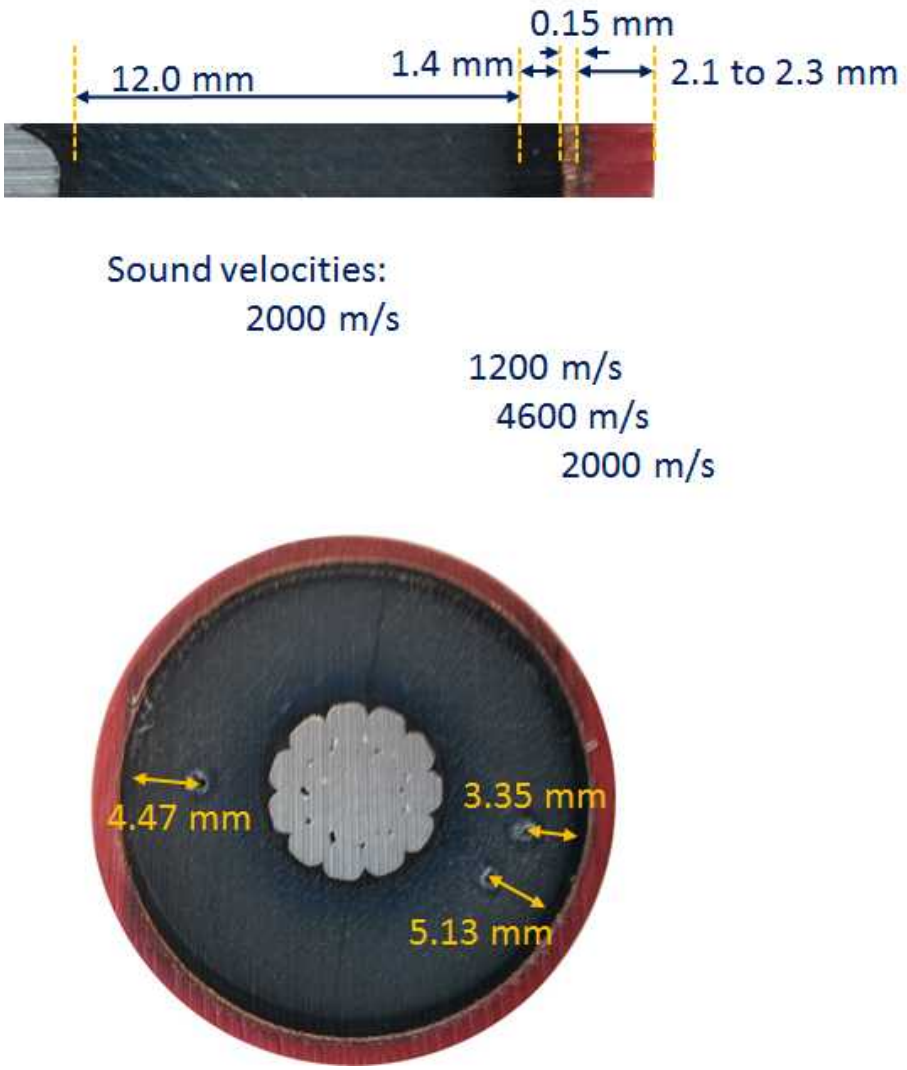

Figure 4.14: Picture of the cable under test as well as the measured sound velocities of the different layers that are on top of the XLPE insulation.

protective layers and XLPE can be calculated by $4.4/(2000\times10^3\times2\times10^{-8})+0.3/(4600\times10^3\times2\times10^{-8})+2.8/(2000\times10^3\times2\times10^{-8}) = 230$ and $24/(2000\times10^3\times2\times10^{-8}) = 600$ respectively.

Having identified the number of samples within the XLPE area, we concentrated our efforts on the specific area instead of the whole original scan. Figure 4.15 (a) shows a ultrasound B scan image formed by collecting all the scans around the red XLPE power cable. Obviously, we can see that there are some samples with very high amplitude in position 14, 17 and 37, where there is a fault located within the Line of Sight (LOS) of

the transducer, as shown in Figure 4.15 (b)(c)(d). In order to distinguish the three positions from the others, a threshold was designed to compare the amplitude of the original returned signal. From Figure 4.16, we can see that the threshold was set to 0.08, except for the peaks of position 14, 17 and 37, none of the other peaks reache this threshold.

Another metric was used to confirm the presence of a fault based on the energy calculated at the surrounding original samples of the strongest peak as highlighted in the circles shown in Figure 4.17. As the transmitted waveform used was a single cycle of a sinusoid, the expectation is that these areas would have a strong signature in the return waveform; otherwise that peak was to be considered noise. The highlighted ellipses show the only regions were the thresholds rendered an indication of a fault.

In addition, we conducted experiments on the good cable and analyzed the received scans in the same way. The ultrasound image is illustrated with the same colorbar scale, as shown in Figure 4.18. Also, from Figure 4.19, we can see that no peaks reached the threshold 0.08.

4.4.2 The Results Based on Fourth-order Cumulants

The fourth-order cumulants were estimated by using the higher order spectrum analysis toolbox. Figure 4.20 shows the fourth-order cumulants results of position 4 and position 20 with no faults in the LOS of transducer, position 14 with two holes in the LOS of transducer and position 37 with one hole in the LOS of transducer. Same colorbar was used to make the comparison clearer. Obviously, the result of position 37 has the strongest intensity. From Figure 4.21, we can see the peaks of fourth-order cumulants results of 48 scans for the faulty cable. The peak of scan 37 is considerably higher than the others. However, the peak of scan 14 is slightly higher and the peak of scan 17 is even lower than some others. The reason is that the two holes are very close, as shown in Figure 4.15, which made it possible for received waves to add destructively. However, for scan 37, it can be seen from Figure 4.22 that the energy at the surrounding original samples of the strongest peak is also very strong.

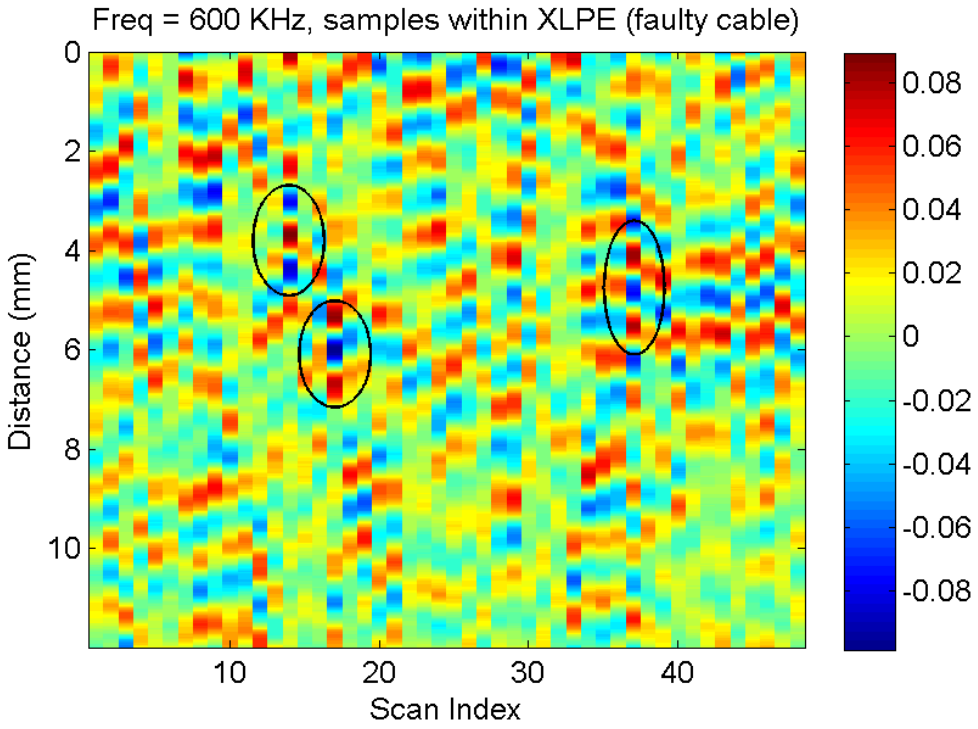

(a)

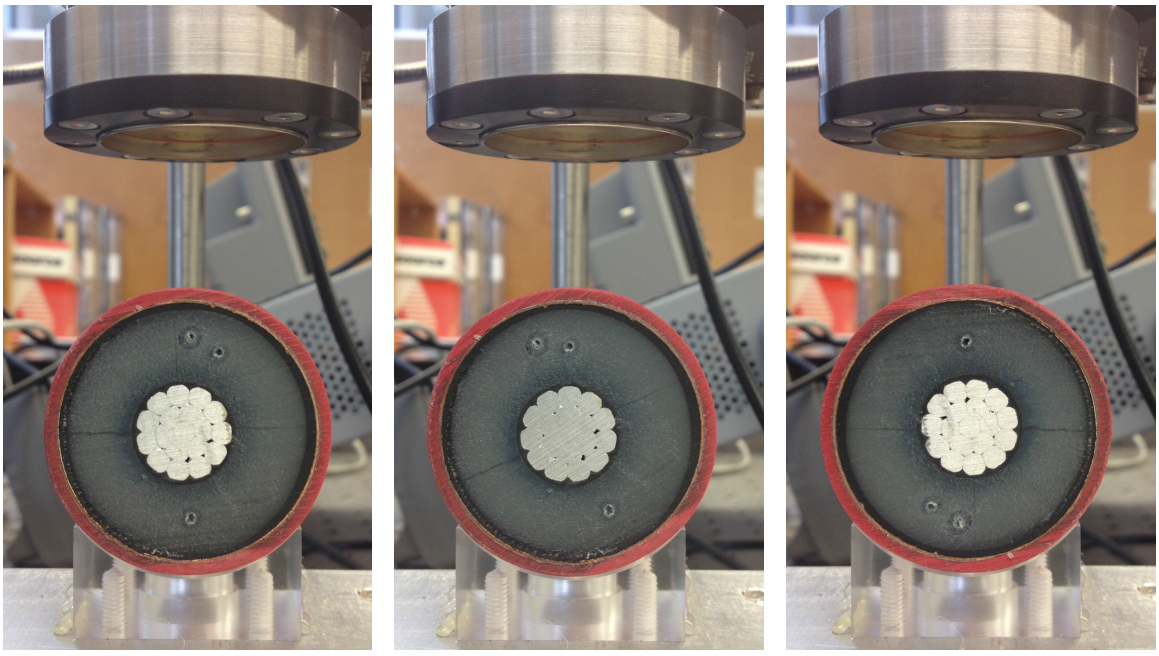

(b) (c) (d)

Figure 4.15: (a) Samples within XLPE area. (b) Position14. (c)Position 17. (d)Position 37.

Figure 4.23 shows two ultrasound scans of position 37 where a fault is in the LOS and position 21 where there is no fault. As it can be seen, the maximum peak where no fault is

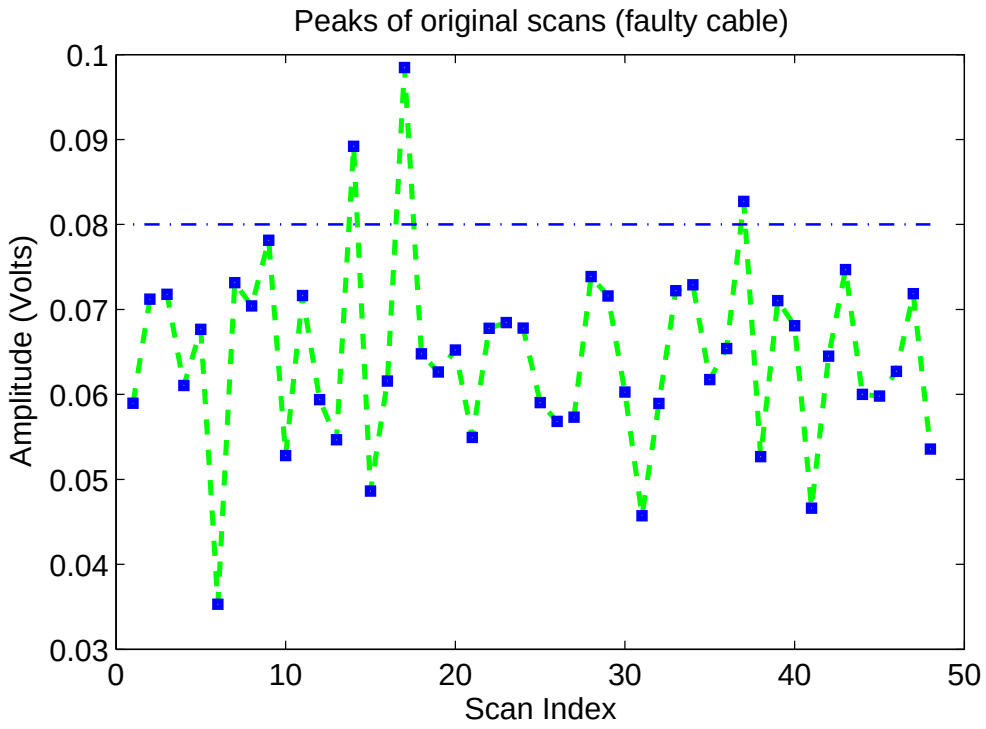

Figure 4.16: Peaks of the original data for the 48 scans (faulty cable). Except for the peaks of position 14, 17 and 37, none of the other peaks reaches the threshold 0.08.

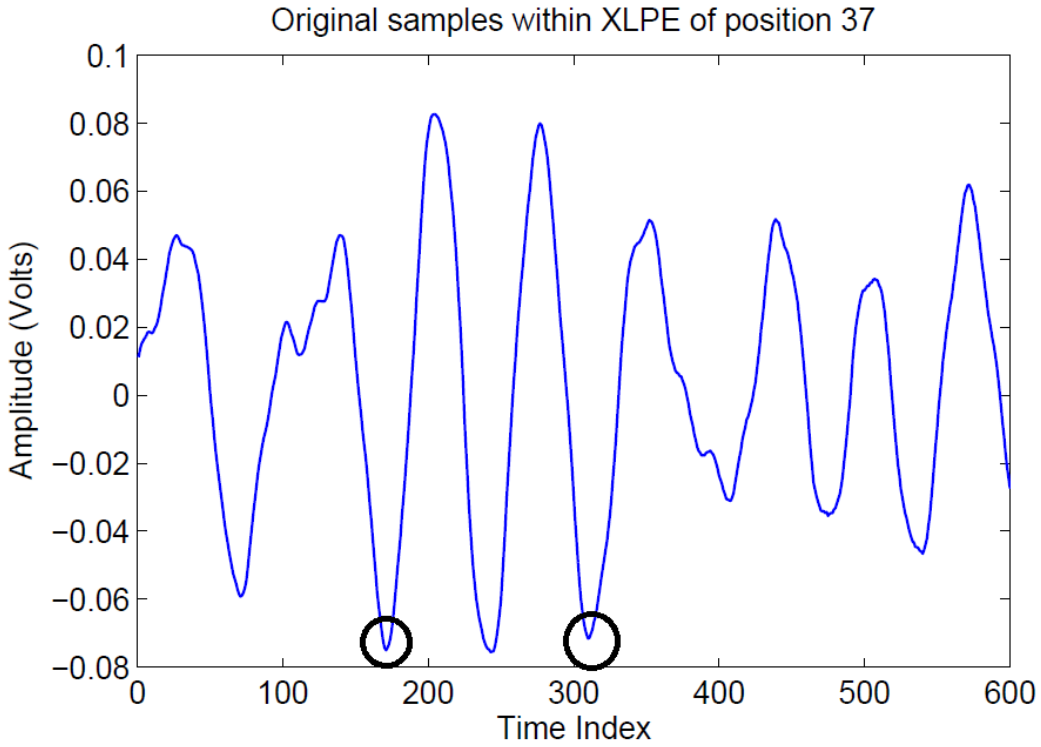

Figure 4.17: Original samples within XLPE of position 37.

Algorithm 3 Illustrate the ultrasound images.

```
N1 = 230;
N2 = 600;
BadCableAll = zeros(10000,48);
BadCableZoom = zeros(N2,48);
BadXLPEMax = zeros(48,1);
counter = 1;
for i = 1001:1048; do
    dataName = ['bad',num2str(i),'.csv'];
    a1 = xlsread(dataName);
    BadCableAll(:,counter) = a1;
    pos1 = find(abs(BadCableAll(2901:3100,counter)) ==
    max(abs(BadCableAll(2901:3100,counter))));
    pos(counter) = pos1(1) + 2900;
    BadCableZoom(:,counter) = BadCableAll(pos(counter)+N1+1:pos(counter)+N1+N2,counter);
    BadXLPEMax(counter) = max(abs(BadCableZoom(:,counter)));
    counter = counter + 1;
end for
figure
imagesc(BadCableAll)
title('Original scans with first highest amplitudes')
for i = 1:counter-1 do
    text(i,pos(i),'o')
end for
figure
x = 1:48;
distawithinXLPE = 0:600-1;
distawithinXLPE = 0.5 ×distawithinXLPE.∗2 × 10^−8. × 2. × 10^6;
imagesc(x,distawithinXLPE,BadCableZoom);
title('Freq = 600 KHz, samples within XLPE (faulty cable)')
figure
plot(x,BadXLPEMax, '–gs','LineWidth',2,'MarkerSize',3,'MarkerEdgeColor','b',
'MarkerFaceColor',[0.5,0.5,0.5]);
title('Peaks of original scans (faulty cable)');
```

presence is considerably low, only 3.56 decibels below the strongest peak of the other scan that detected the fault. By introducing the use of the fourth-order spectrum, we obtained the results shown in Figure 4.20. The maximum peak value levels on the fourth-order cumulants between both cases have a difference of 11.23 decibels. On average using the original ultrasound scans, the strongest peak where the fault is located is 2.59 dB above the other peaks and is 16.55 dB for fourth-order cumulants. Thus thresholding the fourth-order

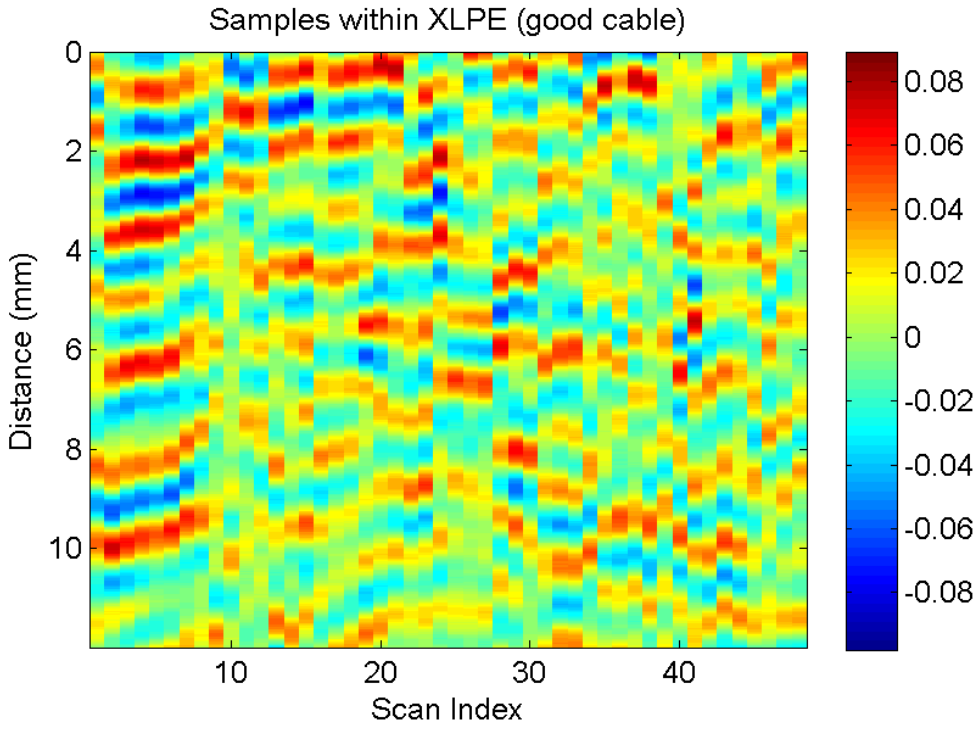

Figure 4.18: Samples of original received signal within XLPE for good cable.

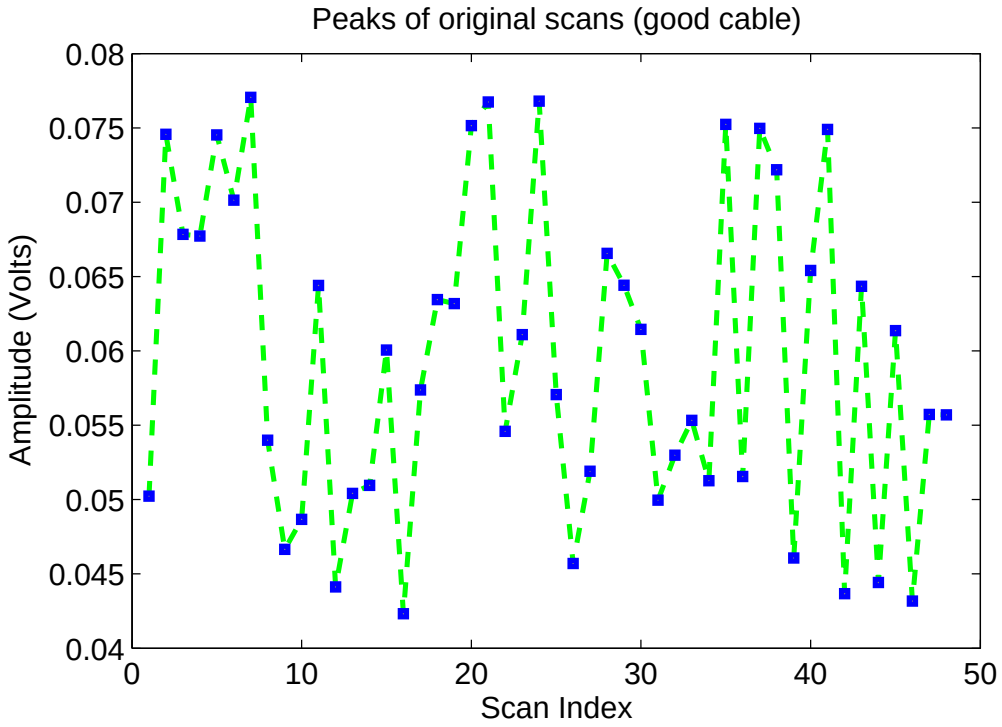

Figure 4.19: Peaks of the original data for the 48 scans (good cable). None of the peaks reaches the threshold 0.08.

spectrum is easier than using the original data.

Fourth-order cumulants was applied to the good cable as well and Figure 4.24 indicates the peaks of fourth-order cumulants results. None of the peaks reaches the threshold 1e-6.

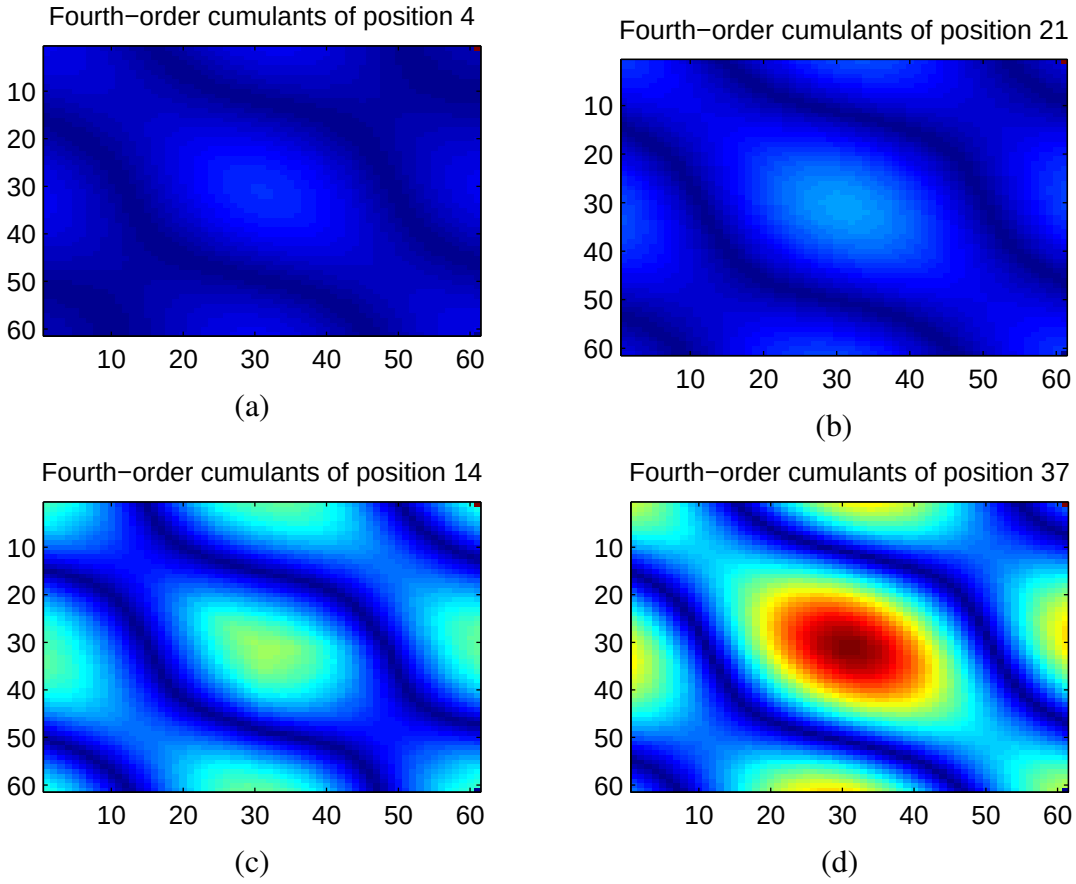

Figure 4.20: (a)(b) Fourth-order cumulants of received signal from position 4 and position 21 with no faults in the LOS of transducer. (c) Fourth-order cumulants of received signal from position 14 where there are 2 holes in the LOS of transducer. (d)Fourth-order cumulants of received signal from position 37 where there is 1 hole in the LOS of transducer.

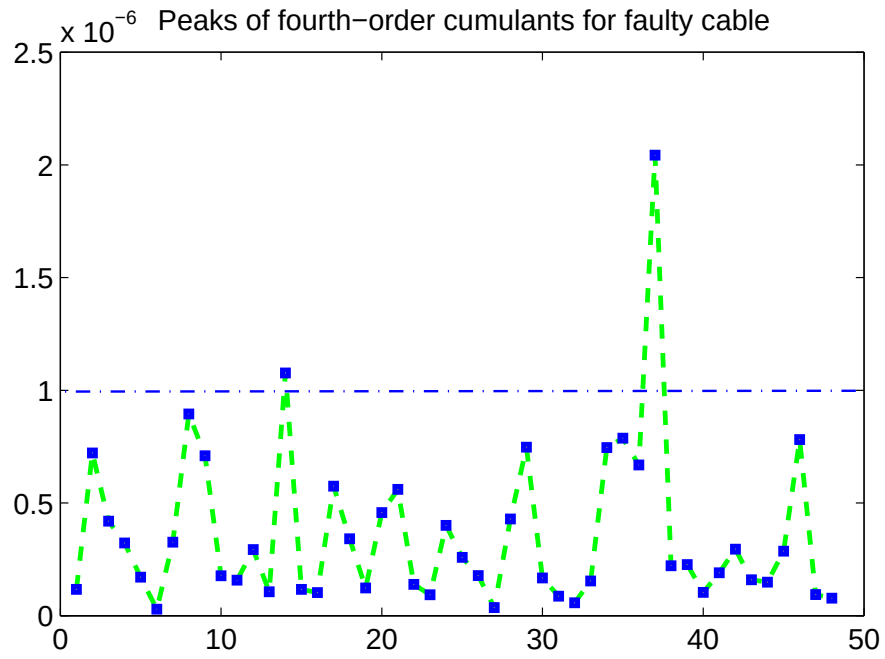

Figure 4.21: Peaks of fourth-order cumulants of 48 scans for the faulty cable.

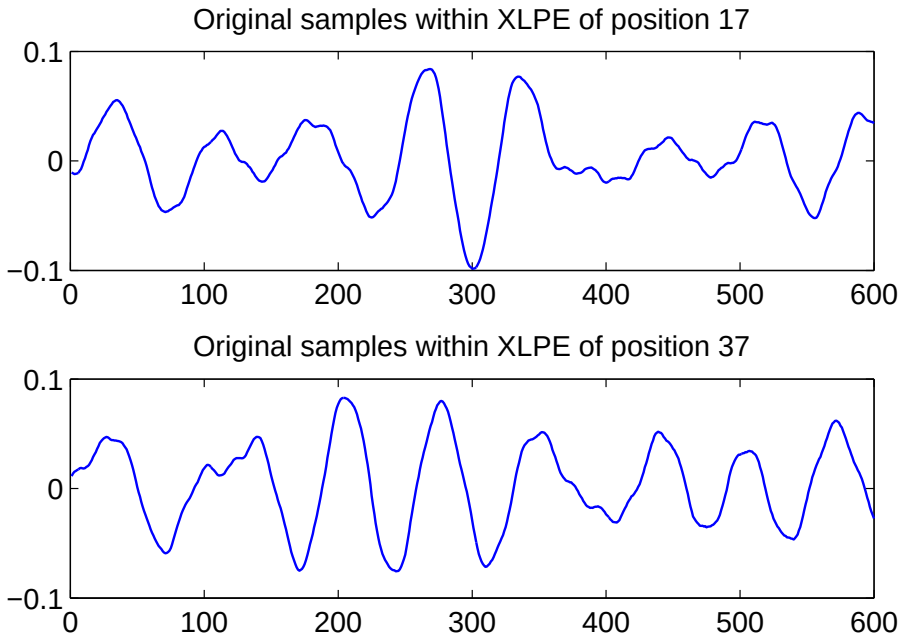

Figure 4.22: Original samples within XLPE of position 17 with two holes in the LOS of transducer and original samples within XLPE of position 37 with one hole in the LOS of transducer.

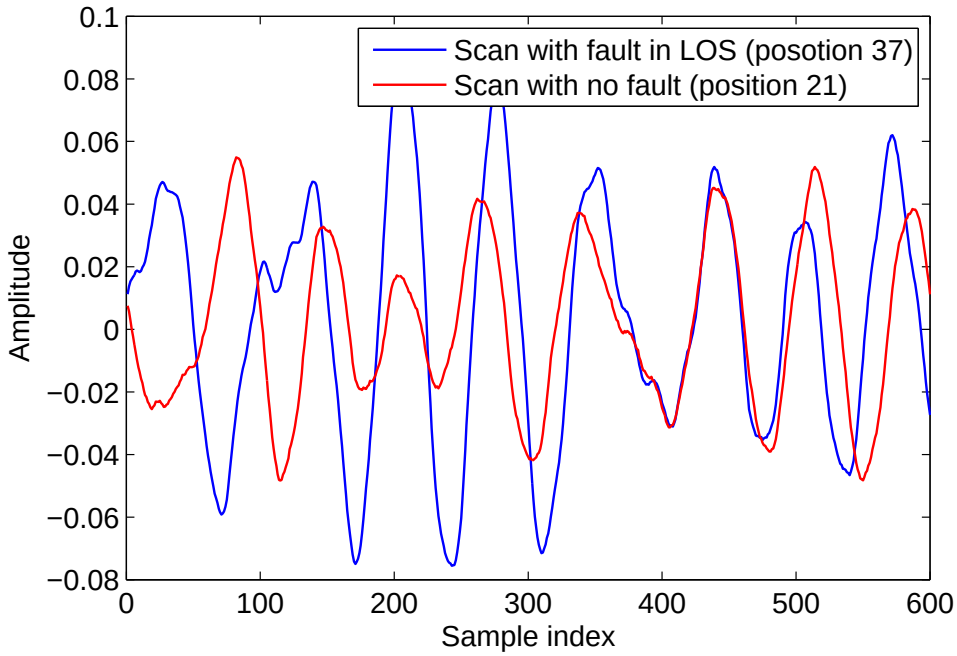

Figure 4.23: Original scans of position 21 (no hole) and position 37 (one hole). The peak of scan 37 is 3.56 decibels higher than the peak of scan 21.

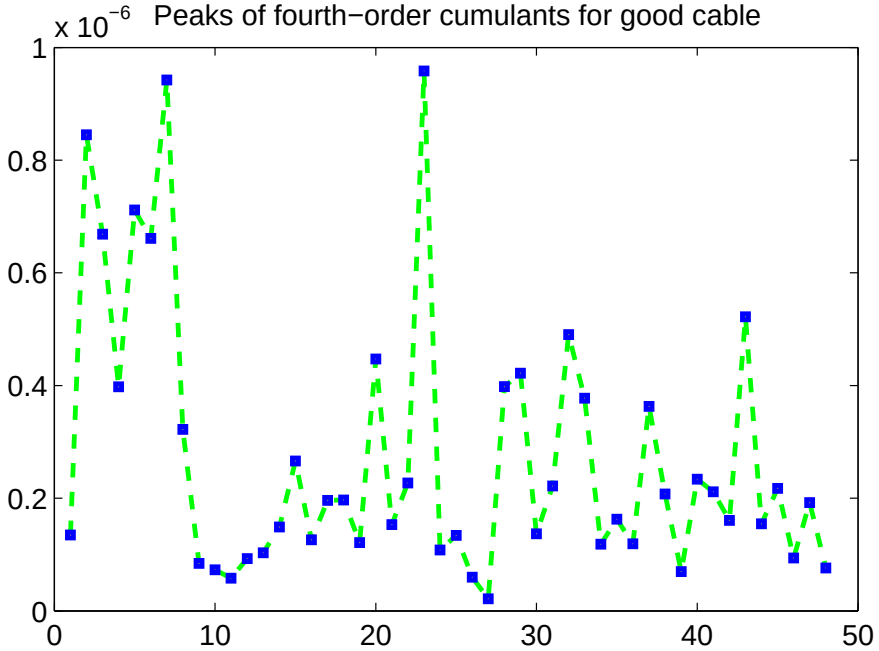

Figure 4.24: Peaks of fourth-order cumulants results of 48 scans for the good cable

Algorithm 4 Fourth-order Cumulants Analysis

```
load badCableData
BadCableZoom1 = BadCableZoom';
peakHOS = zeros(48,1);
n = 30;
[s1 s2] = size(BadCableZoom1);
result = zeros(s1,2*n+1,2*n+1);
for i = 1:s1 do
    for k = -n:n do
        cmat(:,k+n+1) = cumest(BadCableZoom4(i,1:end),4,n,600,0,'biased',k);
    end for
    result(i,:,:) = cmat;
end for
maxvalue = max(max(max(abs(result))));
for i = 1:48 do
    a1 = result(i,:,:);
    peakHos(i) = max(max(abs(a1)));
    a1 = reshape(a1,2*n+1,2*n+1);
    a1(1,2*n+1) = maxvalue;
    a1(2*n+1,2*n+1) = 0;
    figure
    a2 = abs(a1);
    imagesc(a2)
    title(['Fourth-order cumulants of position ', num2str(i)]);
end for
figure
x = 1:48;
plot(x,peakHOS,'–gs','LineWidth',2,'MarkerSize',3,'MarkerEdgeColor','b','MarkerFaceColor',
[0.5,0.5,0.5])
title('Peaks of fourth-order cumulants for faulty cable');
```

Chapter 5

Conclusions and Future Work

5.1 Conclusion and Comments

In this thesis, the cable insulation materials, faults and techniques for detecting faults in XLPE power cables were reviewed. We focused on non-destructive testing based on ultrasound images and the fourth-order spectra.

In Chapter 2, the knowledge of non-destructive testing using ultrasound was discussed. Due to the impedance mismatch in different materials, reflection occurs when ultrasound penetrates into various mediums and the transmission coefficient is determined by the acoustic impedances. Based on that, NDT was employed in this work. Ultrasound is transmitted and received with an ultrasonic transducer. Compared with other transducers, capacitive transducer has a range of advantages, hence, it was used in this thesis. The operating frequency was decided based on the theory that the lowest size of the flaw that can be detected is one-half wavelength.

In Chapter 3, the higher order spectral analysis was described. Compared with power spectrum, it not only contains more information, but also maintain high signal-to-noise ratio. The third-order cumulant and the fourth-order cumulant were compared and the fourth-order cumulant was found to be better for this application.

In Chapter 4, a new non-destructive method of fault detection on XLPE power cables

based on ultrasound images and fourth-cumulant was proposed. The main instrument used in this work was a capacitive transducer with center frequency of 802.8 KHz. A good sample and a faulty sample with three small holes were tested for collecting data. Based on the received scan, the first peak was considered to be the surface of the cable. Then the amplitude peaks of the samples within XLPE were compared by setting a threshold of 0.08 Volts. None of the peaks except those of the tree positions with fault in the LOS of the transducer. Also, the fourth-order cumulant was applied to further locate the faults. The result of the position with one hole in the LOS of the transducer turned out to have much higher amplitude. However, it was very difficult to distinguish the position with two holes from others, because the two holes were very close.

5.2 Future Work

In our proposed method for locating water trees in XLPE power cables, the position of transducer was adjusted very carefully when collecting data to make sure that the transducer was orthogonal to the surface of the power cable. However, the surface of the power cable is not perfectly smooth. Instead, there are a lot of bumps. Besides, the surface of the outer protective layer could be damaged after the cable buried underground for a few years. For some cables, the thickness of each layer is slightly different, and there are even some overlaps. All the challenges make it complicated to detect water trees in XLPE power cables in practice.

Furthermore, the water trees were only simulated by drilling small holes in the XLPE power cables. However, the substances in the water trees of filed-aged cables are much different. Various investigators have found that the water trees consist of carbonyl, metal ions and water, even though further effort is still required to completely understand this phenomenon. Even if the water drys out after the cables are exposed in air, the content in water trees is still complex. Therefore, the reflection coefficient at the XLPE-water tree boundary is much different as the refection coefficient at the XLPE-air boundary, which

makes it more difficult to locate the faults from the received scans. As we have discussed before, the operating frequency of the ultrasonic transducer is chosen mainly based on the size of the faults to be detected. Hence, a transducer with much higher frequency is required for detecting the field-aged cables. Also, many water trees can be close to each other, and a transducer with higher frequency is preferable. However, at higher frequencies, attenuation increases with frequency. In future work, experiments can be conducted on the field-aged cables with real water trees to further prove the method proposed in this thesis.

Reference

[1] I. A. Metwally, "The evolution of medium voltage power cables," *Potentials, IEEE*, vol. 31, no. 3, pp. 20–25, 2012.

[2] "Cable insulation materials," Nov 2012. [Online]. Available: http://www.openelectrical.org/wiki/index.php?title=Cable_Insulation_Materials

[3] S. Ma, J. Lu, and J. Gao, "Study of the low temperature pyrolysis of pvc," *Energy & Fuels*, vol. 16, no. 2, pp. 338–342, 2002.

[4] E. Reeves and M. J. Heathcote, *Newnes electrical pocket book*. Copyright licensing adency ltd, 2003.

[5] T. Miyashita, "Deterioration of water-immersed polyethylene-coated wire by treeing," *Electrical Insulation, IEEE Transactions on*, vol. EI-6, no. 3, pp. 129–135, Sept 1971.

[6] J. Xu and S. Boggs, "The chemical nature of water treeing: theories and evidence," *Electrical Insulation Magazine, IEEE*, vol. 10, no. 5, pp. 29–37, Sept 1994.

[7] R. Ross, "Inception and propagation mechanisms of water treeing," *Dielectrics and Electrical Insulation, IEEE Transactions on*, vol. 5, no. 5, pp. 660–680, Oct 1998.

[8] A. Garton, S. Bamji, A. Bulinski, and J. Densley, "Oxidation and water tree formation in service-aged xlpe cable insulation," *Electrical Insulation, IEEE Transactions on*, vol. EI-22, no. 4, pp. 405–412, Aug 1987.

[9] H.-J. Henkel, N. Muller, J. Nordmann, W. Rogler, and W. Rose, "Relationship between the chemical structure and the effectiveness of additives in inhibiting water-trees," *Electrical Insulation, IEEE Transactions on*, vol. EI-22, no. 2, pp. 157–161, April 1987.

[10] E. Steennis and F. Kreuger, "Water treeing in polyethylene cables," *Electrical Insulation, IEEE Transactions on*, vol. 25, no. 5, pp. 989–1028, Oct 1990.

[11] H. Faremo, M. Selsjord, S. Hvidsten, K. M. Bengtsson, and A. Ryen, "Initiation of vented water trees from the conductor screen of mv xlpe insulated cables," in *Electrical Insulation (ISEI), Conference Record of the 2012 IEEE International Symposium on*. IEEE, 2012, pp. 386–390.

[12] M. Shaw and S. Shaw, "Water treeing in solid dielectrics," *Electrical Insulation, IEEE Transactions on*, vol. EI-19, no. 5, pp. 419–452, Oct 1984.

[13] T. Fukuda, S. Suzuki, and Y. Nitta, "Water trees in 3.3 and 6.6 kv cross-linked polyethylene power cables," in *Annual report of the NAS conference on elctrical insulation and electric phenomena*, 1972, pp. 211–215.

[14] C. Meyer, "Water absorption during water treeing in polyethylene," *Electrical Insulation, IEEE Transactions on*, vol. 1, no. E1-18, pp. 28–31, 1983.

[15] J. Filippini, Y. Poggi, and J. Viard, "Water tree induced breakdown in polyethylene," in *Conduction and Breakdown in Solid Dielectrics, 1992., Proceedings of the 4th International Conference on*, Jun 1992, pp. 358–362.

[16] G. Thomas, D. Flores-Tapia, S. Pistorius, and N. Fernando, "Synthetic aperture ultrasound imaging of XLPE insulation of underground power cables," *IEEE Electrical Insulation Magazine*, vol. 3, no. 26, pp. 24–34.

[17] V. Honkimki, K. Hmlinen, and S. Manninen, "Quantitative x-ray fluorescence analysis using fundamental parameters: Application to gold jewelry," *X-Ray Spectrometry*, vol. 25, no. 5, pp. 215–220, 1996. [Online]. Available: http://dx.doi.org/10.1002/(SICI)1097-4539(199609)25:5⟨215::AID-XRS165⟩3.0.CO;2-Z

[18] R. Schurch, S. Rowland, R. Bradley, and P. Withers, "Imaging and analysis techniques for electrical trees using x-ray computed tomography," *Dielectrics and Electrical Insulation, IEEE Transactions on*, vol. 21, no. 1, pp. 53–63, February 2014.

[19] Y. Zhu, G. Tian, R. Lu, and H. Zhang, "A review of optical ndt technologies," *Sensors*, vol. 11, no. 8, pp. 7773–7798, August 2011.

[20] F. Weigand, H. Spiess, B. Blumich, G. Salge, and K. Moller, "Nuclear magnetic resonance imaging of electrical trees in pe," *Dielectrics and electrical insulation, IEEE Transactions on*, vol. 4, no. 3, pp. 280–285, 1997.

[21] D. Auckland, C. Smith, and B. Varlow, "Application of ultrasound to the ndt of solid insulation," *Science, Measurement and Technology, IEE Proceedings*, vol. 141, no. 1, pp. 20–24, Jan 1994.

[22] D. Auckland, A. McGrail, C. Smith, B. Varlow, J. Zhao, and D. Zhu, "Application of ultrasound to the inspection of insulation," *Science, Measurement and Technology, IEE Proceedings* -, vol. 143, no. 3, pp. 177–181, May 1996.

[23] D. Auckland, A. McGrail, C. Smith, and B. Varlow, "The use of ultrasound for the detection of water trees in xlpe cable," in *Conduction and Breakdown in Solid Dielectrics, 1995. ICSD'95., Proceedings of the 1995 IEEE 5th International Conference on*, Jul 1995, pp. 681–684.

[24] E. Blomme, D. Bulcaen, and F. Declercq, "Air-coupled ultrasonic nde: experiments in the frequency range 750 khz2 MHz," *NDT and E International*, vol. 35, no. 7, pp. 417–426, 2002.

[25] R. Berg and D. Stock, *The physics of sound*. Pearson Education India, 1982.

[26] D. Lazarus, "The variation of the adiabatic elastic constants of kcl, nacl, cuzn, cu, and al with pressure to 10,000 bars," *Phys. Rev.*, vol. 76, pp. 545–553, Aug 1949. [Online]. Available: http://link.aps.org/doi/10.1103/PhysRev.76.545

[27] S. Klima and J. Freche, "Ultrasonic detection and measurement of fatigue cracks in notched specimens," *Experimental Mechanics*, vol. 9, no. 5, pp. 193–202, 1969. [Online]. Available: http://dx.doi.org/10.1007/BF02326535

[28] Y. Q. Guo and D. N. Fang, "Formation of longitudinal wave band structures in one-dimensional phononic crystals," *Journal of Applied Physics*, vol. 109, no. 7, 2011. [Online]. Available: http://scitation.aip.org/content/aip/journal/jap/109/7/10.1063/1.3567911

[29] C. Liner, *Elements of Seismic Dispersion: A Somewhat Practical Guide to Frequency-dependent Phenomena*. Society of Exploration Geophysicists, 2012.

[30] I. Viktorov, *Rayleigh and Lamb Waves*. Plenum Press New York, 1967.

[31] J. Blitz and G. Simpson, *Ultrasonic Methods of Non-destructive Testing*. Chapman & Hall, 1996.

[32] W. P. Mason, "Physical acoustics and the properties of solids," *The Journal of the Acoustical Society of America*, vol. 28, no. 6, 1956.

[33] G. D. Ludwig, "The velocity of sound through tissues and the acoustic impedance of tissues," *The Journal of the Acoustical Society of America*, vol. 22, no. 6, 1950.

[34] D. Z. Reinstein, R. H. Silverman, and D. J. Coleman, "High-frequency ultrasound measurement of the thickness of the corneal epithelium," *Refractive and corneal surgery*, vol. 9, pp. 385–385, 1993.

[35] J. Blitz and G. Simpson, *Ultrasonic methods of non-destructive testing*. Springer Science & Business Media, 1996, vol. 2.

[36] G. Thomas, A. Emadi, J. Mijares-Chan, and D. A. Buchanan, "Low frequency ultrasound ndt of power cable insulation," in *Instrumentation and Measurement Technology Conference (I2MTC) Proceedings, 2014 IEEE International*. IEEE, 2014, pp. 1126–1129.

[37] G. Hashmi, R. Papazyan, and M. Lehtonen, "Determining wave propagation characteristics of mv xlpe power cable using time domain reflectometry technique," in *Electrical and Electronics Engineering, 2009. ELECO 2009. International Conference on*, Nov 2009, pp. I–159–I–163.

[38] W. Grandia and C. Fortunko, "NDT applications of air-coupled ultrasonic transducers," in *Ultrasonics Symposium, 1995. Proceedings., 1995 IEEE*, vol. 1. IEEE, 1995, pp. 697–709.

[39] W. Manthey, N. Kroemer, and V. Magori, "Ultrasonic transducers and transducer arrays for applications in air," *Measurement Science and Technology*, vol. 3, no. 3, pp. 249–262, 1992.

[40] D. A. Berlincourt, D. R. Curran, and H. Jaffe, "Piezoelectric and piezomagnetic materials and their function in transducers," *Physical Acoustics: Principles and Methods*, vol. 1, no. Part A, p. 247, 1964.

[41] J. T. Bushberg, J. A. Seibert, E. M. Leidholdt Jr, and J. M. Boone, *The essential physics of medical imaging*. Lippincott Williams & Wilkins, 2011.

[42] D. Schindel, D. Hutchins, and W. Grandia, "Capacitive and piezoelectric air-coupled transducers for resonant ultrasonic inspection," *Ultrasonics*, vol. 34, no. 6, pp. 621 – 627, 1996. [Online]. Available: http://www.sciencedirect.com/science/article/pii/0041624X96000637

[43] W. Manthey, N. Kroemer, and V. Magori, "Ultrasonic transducers and transducer arrays for applications in air," *Measurement Science and Technology*, vol. 3, no. 3, p. 249, 1992. [Online]. Available: http://stacks.iop.org/0957-0233/3/i=3/a=001

[44] W. Munro, S. Pomeroy, M. Rafiq, H. Williams, M. Wybrow, and C. Wykes, "Ultrasonic vehicle guidance transducer," *Ultrasonics*, vol. 28, no. 6, pp. 350 – 354, 1990. [Online]. Available: http://www.sciencedirect.com/science/article/pii/0041624X9090054R

[45] S. S. Kallempudi and Y. Gurbuz, "A nanostructured-nickel based interdigitated capacitive transducer for biosensor applications," *Sensors and Actuators B: Chemical*, vol. 160, no. 1, pp. 891 – 898, 2011. [Online]. Available: http://www.sciencedirect.com/science/article/pii/S092540051100801X

[46] M. Shin, J. S. Krause, P. DeBitetto, and R. D. White, "Acoustic doppler velocity measurement system using capacitive micromachined ultrasound transducer array technology," *The Journal of the Acoustical Society of America*, vol. 134, no. 2, 2013.

[47] A. Robbins and W. Miller, *Circuit analysis: Theory and practice*. Delmar, 2000.

[48] R. Serway, R. Beichner, and J. Jewett, *Physics for Scientists and Engineers*. Fort Worth: Saunders College Publishing, 2000.

[49] J. I. Seeger and B. E. Boser, "Dynamics and control of parallel-plate actuators beyond the electrostatic instability," in *Transducers*, vol. 99. Citeseer, 1999, pp. 474–477.

[50] M. Buttiker, "Capacitance, admittance, and rectification properties of small conductors," *Journal of Physics: Condensed Matter*, vol. 5, no. 50, p. 9361, 1993.

[51] O. Vatel and M. Tanimoto, "Kelvin probe force microscopy for potential distribution measurement of semiconductor devices," *Journal of applied physics*, vol. 77, no. 6, pp. 2358–2362, 1995.

[52] S. K. Chakarvarti, "Permittivity of free space and dielectric constant measurement," *The Physics Teacher*, vol. 19, no. 2, 1981.

[53] W. Benenson, H. Stoecker, W. Harris, and H. Lutz, *Handbook of Physics*. New York: Springer, 2002.

[54] B. Kumar, G. Rajita, and N. Mandal, "A review on capacitive-type sensor for measurement of height of liquid level," *Measurement and Control*, vol. 47, no. 7, pp. 219–224, 2014.

[55] J. Novak and J. Feddema, "A capacitance-based proximity sensor for whole arm obstacle avoidance," in *Robotics and Automation, 1992. Proceedings., 1992 IEEE International Conference on*, vol. 2, May 1992, pp. 1307–1314.

[56] N. I. Andermo, "Capacitance-type measuring device for absolute measurement of positions," Nov 1989, uS patent 4,879,508.

[57] U. Kang and K. D. Wise, "A high-speed capacitive humidity sensor with on-chip thermal reset," *Electron Devices, IEEE Transactions on*, vol. 47, no. 4, pp. 702–710, 2000.

[58] L. Zhao and E. Yeatman, "Micro capacitive tilt sensor for human body movement detection," in *4th International Workshop on Wearable and Implantable Body Sensor Networks (BSN 2007)*, 2007, pp. 195–200.

[59] "Data presentation." [Online]. Available: http://www.nde-ed.org/EducationResources/CommunityCollege/Ultrasonics/EquipmentTrans/DataPres.htm

[60] V. Bindal, *Transducers for Ultrasonic Flaw Detection*. Narosa Publishing House, 1999.

[61] J. Lamperti, *Stochastic Processes*. New York: Springer, 1977.

[62] A. Fung, "A note on the wiener-khintchine theorem for autocorrelation," *Proceedings of the IEEE*, vol. 55, no. 4, pp. 594–595, 1967.

[63] C. Nikias and A. Petropulu, *Higher-Order Spectra Analysis: A Nonlinear Signal Processing Framework*. PTR Prentice Hall, 1993.

[64] A. Swami and J. Mendel, "Cumulant-based approach to harmonic retrieval and related problems," *Signal Processing, IEEE Transactions on*, vol. 39, no. 5, pp. 1099–1109, May 1991.

[65] R. Kumaresan and D. Tufts, "Estimating the angles of arrival of multiple plane waves," *Aerospace and Electronic Systems, IEEE Transactions on*, vol. AES-19, no. 1, pp. 134–139, Jan 1983.

[66] C. Klüppelberg and T. Mikosch, "Some limit theory for the self-normalised periodogram of stable processes," *Scandinavian Journal of Statistics*, pp. 485–491, 1994.

[67] J. Liu and P. Wu, "Higher order spectra denoising method of phase matching noise estimation," in *Pervasive Computing Signal Processing and Applications (PCSPA), 2010 First International Conference on*. IEEE, 2010, pp. 811–814.

[68] A. Masson, B. Shishkov, and F. Lefeuvre, "On the use of high order statistical tests of the analysis of time series associated with space data," *Traitement du Signal*, pp. 59–78, 2001.

[69] S. Wan, B. Raju, and M. Srinivasan, "Robust deconvolution of high-frequency ultrasound images using higher-order spectral analysis and wavelets," *Ultrasonics, Ferroelectrics and Frequency Control, IEEE Transactions on*, vol. 50, no. 10, pp. 1286–1295, 2003.

[70] T. Taxt, "Comparison of cepstrum-based methods for radial blind deconvolution of ultrasound images," *Ultrasonics, Ferroelectrics, and Frequency Control, IEEE Transactions on*, vol. 44, no. 3, pp. 666–674, May 1997.

[71] J. De la Rosa, I. Lloret, A. Moreno, R. Piotrkowski, J. Ruzzante, C. G. Puntonet, and J. Górriz, "Higher-order spectra and independent component analysis used for identification and snr enhancement of acoustic emission signals," in *Electrotechnical Conference, 2006. MELECON 2006. IEEE Mediterranean*. IEEE, 2006, pp. 490–493.

[72] Z. Jiang, B. L. Luk, and K. Liu, "Bispectra-based impact acoustic non-destructive evaluation," *NDT & E International*, vol. 42, no. 7, pp. 652–657, 2009.